Journal of Controlled Release 329 (2021) 570–584

Contents lists available at ScienceDirect

Journal of Controlled Release

journal homepage: www.elsevier.com/locate/jconrel

Analysis of the bone fracture targeting properties of osteotropic ligands

Jeffery J. Nielsen [a], Stewart A. Low [b], Neal T. Ramseier [b], Rahul V. Hadap [b], Nicholas A. Young [a], Mingding Wang [b], Philip S. Low [a,b,*]

[a] Department of Medicinal Chemistry and Molecular Pharmacology, Purdue University, West Lafayette, IN, United States of America
[b] Department of Chemistry, Purdue University, West Lafayette, IN, United States of America

ARTICLE INFO

Keywords:
Acidic oligopeptides
Bone fracture targeting ligands
Targeted drug delivery
Acceleration of fracture healing
Osteogenic therapies
Bisphosphonates

ABSTRACT

Purpose: Although more than 18,000,000 fractures occur each year in the US, methods to promote fracture healing still rely primarily on fracture stabilization, with use of bone anabolic agents to accelerate fracture repair limited to rare occasions when the agent can be applied to the fracture surface. Because management of broken bones could be improved if bone anabolic agents could be continuously applied to a fracture over the entire course of the healing process, we undertook to identify strategies that would allow selective concentration of bone anabolic agents on a fracture surface following systemic administration. Moreover, because hydroxyapatite is uniquely exposed on a broken bone, we searched for molecules that would bind with high affinity and specificity for hydroxyapatite. We envisioned that by conjugating such osteotropic ligands to a bone anabolic agent, we could acquire the ability to continuously stimulate fracture healing.

Results: Although bisphosphonates and tetracyclines were capable of localizing small amounts of peptidic payloads to fracture surfaces 2-fold over healthy bone, their specificities and capacities for drug delivery were significantly inferior to subsequent other ligands, and were therefore considered no further. In contrast, short oligopeptides of acidic amino acids were found to localize a peptide payload to a bone fracture 91.9 times more than the control untargeted peptide payload. Furthermore acidic oligopeptides were observed to be capable of targeting all classes of peptides, including hydrophobic, neutral, cationic, anionic, short oligopeptides, and long polypeptides. We further found that highly specific bone fracture targeting of multiple peptidic cargoes can be achieved by subcutaneous injection of the construct.

Conclusions: Using similar constructs, we anticipate that healing of bone fractures in humans that have relied on immobilization alone can be greatly enhanced by continuous stimulation of bone growth using systemic administration of fracture-targeted bone anabolic agents.

1. Introduction

More than 18.3 million bone fractures occur each year in the United States. While uncomplicated fractures may lead to compromised physical activity, loss of productivity, and decreased quality of life [1], nonunion fractures can amplify these morbidities by greatly prolonging the time to recovery [2]. Craniofacial fractures can be especially debilitating due to concomitant difficulties with eating and speaking [3], and delayed hip fracture healing in the elderly can in many cases result in premature mortality [2]. Taken together, the total financial impact of broken bones on reparative costs, convalescent expenses, and physical therapies is estimated at $45.8 billion, and these expenses are anticipated to increase as our population continues to age [3].

Although the physical and financial burdens of fractures in the United States have been frequently lamented, methods for treating these fractures have surprisingly not changed significantly in many years, still relying primarily on stabilization with rods, plates, and/or casts and benefitting little from the plethora of bone anabolic agents that have been continuously reported in the literature [4]. Several reasons likely exist for this lack of significant progress. First, all osteogenic drugs approved to date must be topically applied during surgery, and because surgery is not indicated for most fractures, the opportunity to employ these pharmacologic agents has been limited. [5–7] Second, the metabolic turnover of approved bone anabolic agents is relatively fast [8], restricting the duration of their therapeutic benefits to a brief window following topical application [9,10]. Third, leakage of locally-applied anabolic drugs into surrounding tissues can often lead to undesirable side effects, including ectopic bone growth, [10,11] and systemic

* Corresponding author at: 720 Clinic Drive West Lafayette, IN 47907, USA.
E-mail address: plow@purdue.edu (P.S. Low).

https://doi.org/10.1016/j.jconrel.2020.09.047
Received 1 June 2020; Received in revised form 21 September 2020; Accepted 27 September 2020
Available online 6 October 2020

administration of osteogenic agents can stimulate unwanted anabolic processes in healthy tissues such as nerves [12–14], muscles [15,16], and the vasculature [17–19]. Indeed, hypercalcemia [20,21], hypertension [22–24], tachycardia [25,26], immunosuppression [27–30], and even cancer [31,32] are among the concerns surrounding systemic administration of bone anabolic drugs.

Recognizing the benefits that could accrue if continuous application of bone anabolic agents to fracture surfaces were possible, we looked for strategies that might allow systemic administration of osteogenic drugs without causing toxicities to healthy tissues. In this effort, we noted that newlyfractured bones expose hydroxyapatite that is normally covered by a periosteum and endosteum that together limit exposure of the healthy bone to systemically administered drugs [33,34]. We also appreciated that molecules such as bisphosphonates [35–39], tetracyclines [40–42], acidic oligopeptides [43–45], and bone sialoproteins [46–48] naturally localize to exposed hydroxyapatite, suggesting that these and related osteotropic agents might be exploited to deliver attached drugs to fracture surfaces. Many of these have been developed as targeting ligands to deliver small molecules to osteomyelitis [37,49], bone cancers [50–52], or osteoporsis [53–55]. Very little work has been done to develop targeting strategies for delivering therapeutics to bone fractures. Previous work by the Kopecek lab demonstrated the utility of various targeting molecules for different types of hydroxyapatite and demonstrated the ability to use them to deliver anabolic agents to diseased bone [42,56] The Kopecek lab, in collaboration with our lab, developed into the first fracture-targeted anabolic that targets raw hydroxyapatite [57]. This technologyhas proven successful improving the therapeutic efficiency of drugs for healing bone fractures [58,59]. A more in-depth review of the existing bone targeting strategies can be found in the following reviews [60–62]. Encouraged by these observations, we undertook to determine which hydroxyapatite ligand might prove most efficient in targeting anabolic peptides to fractures surfaces. In the paper below, we compare the bone fracturetargeting capabilities of the aforementioned molecules tethered to both imaging agents and bone anabolic peptides of different charges, sizes, and polarities. Our data show that highly acidic oligopeptides constitute the most effective targeting ligands for delivering attached anabolic compounds to fracture surfaces.

2. Materials and methods

2.1. Synthesis of payload peptides

All payloads were briefly synthesized in a solidphase peptide synthesis vial under a stream of argon. Wang resin (0.6 mmol/g) was loaded with 3-fold excess of the first amino acid (cysteine), HOBt-Cl and DIC for 4 h in 9:1 *v*/v CH2Cl2/DMF using catalytic amounts of DMAP. The resin was then capped with 2 equivalents of acetic anhydride and pyridine for 30 min to block any unreacted hydroxyl groups on the resin. These steps were followed by 3 washes with DCM and DMF, consecutively. After each coupling reaction, 9-fluorenylmethoxycarbonyl (Fmoc) groups were removed by two 10-min incubations with 20% (*v*/v) piperidine in DMF. The resin was then washed twice with DMF prior to adding the next amino acid. Each amino acid was reacted in 3-fold excess 2-(1H-benzotriazol-1-yl)-1,1,3,3-tetramethyluronium hexafluorophosphate (HBTU)/*N*-methylmorpholine (NMM) for 30 min, followed by a double coupling with 3-fold excess benzotriazol-1-yl-oxytripyrrolidinophosphonium hexafluorophosphate (PyBOP)/*N*-methylmorpholine (NMM) for 30 min. All amino acids were added according to the conditions above. Standard Fmoc-protected amino acids with acid-sensitive side chain protecting groups were used, unless otherwise noted. Thereafter, tyrosine or the peptide sequence shown in Table 1 was added onto the peptide using the solid-phase procedures listed above using an automated peptide synthesizer (Focus XC, AAPPTec). Upon synthesis completion, the terminal Fmoc was removed using the aforementioned conditions, after which the resin was washed 3 times with DMF, 3 times with DCM, twice with methanol, and then dried with argon gas. The dried resin with the peptide was cleaved using 95:2.5:2.5 trifluoroacetic acid/water/triisopropylsilane and excess TCEP for 2 h. The peptide was then precipitated from the cleavage solution using 10 times the volume of cold diethyl ether. The solution was spun at 2000 RCF for 5 min and then decanted. The pellet was then desiccated and submitted to analytical liquid chromatography–mass spectrometry (1220 LC; 6130 MS, Agilent) for confirmation of synthesis. The crude peptide was dissolved in a mixture of DMF and water and purified via preparative reversed-phase high-performance liquid chromatography (1290, Agilent). A C-18 column with a 0–50% ammonium acetate: acetonitrile mobile phase for 40 min was used to purify the TMP. The fraction that contained only pure payloads as assessed by analytical liquid chromatography–mass spectrometry (1220 LC, 6130 MS, Agilent) was lyophilized(FreeZone, LABCONCO) and stored as lyophilized powder at −20 °C until it was coupled with targeting ligands.

2.2. Synthesis of linear targeting peptides

Targeting ligand peptides were all synthesized to achieve the appropriate length, amino acid composition and enantiomeric stereochemistry, as indicated by their names according to the solid phase synthesis methods described above. While still on the resin, the N-terminal amines were deprotected as described above, and the resin was reacted in DMF with 3-fold maleimide propionic acid, 3-fold excess PYBOP, HOBT-Cl and 5-fold excess DIPEA for 4 h. The peptides were then coupled to the cysteinecontaining peptides using maleimide chemistry in PBS containing 10-fold excess TCEP for 24 h at room temperature. The targeting payload conjugates were then cleaved, deprotected, and purified as described above.

2.3. Synthesis of branched targeting peptides

Briefly, branched targeting ligands were synthesized using solid-phase peptide synthesis under a stream of argon. 2-chlorotrityl resin (0.6 mmol/g) was loaded at 0.6 mmol/g with Nα,Nε-di-Fmoc-L-lysine for 60 min in DCM and DIPEA. The resin was then capped with 4 washes of MeOH, followed by 3 washes with DCM and DMF, consecutively. The branched chain was then synthesized as described above. The N-terminal Fmoc was retained and the peptide was subjected to a soft cleavage

Table 1
The sequences and chemical classes of therapeutic bone anabolic payloads chosen to represent different chemical classes of payloads used to investigate the payloads' role in affecting fracture targeting.

Peptide Payload	Representative Chemical Class	Sequence
F109C-heparin-binding domain of FGF2	Short Oligopeptide	YKRSRYTC
PACAPC-pituitary adenylate cyclase-activating polypeptide	Long Polypeptide	HSDGIFTDSYSRYRKQMAVKKYLAAVLGKRYKQRVKNKC
CTC-C chemotactic cryptic peptide (CTC), derived from the CTX region of collagen type III	Neutral	YIAGVGGEKSGGFYC
Ck2.3C-casein kinase 2 beta chain	Cationic	RQIKIWFQNR RMKWKKIPVG ESLKDLIDQC
ODPC osteopontin-derived peptide	Anionic	DVDVPDGRGDSLAYGC
P4C- BMP-2 fragment	Hydrophobic	KIPKASSVPTELSAISTLYLC

in 1:1:8 mixture of acetic acid/TFE/DCM for 30 min. The cleavage solution was evaporated under reduced pressure and the terminal carboxylic acid was conjugated with 3-fold excess N-(2-aminoethyl) maleimide, 3-fold excess PYBOP and HOBT-Cl and 5-fold excess DIPEA in DCM for 4 h. The acid-sensitive protecting groups were then deprotected by a 2-h incubation in 95:2.5:2.5 trifluoroacetic acid/water/triisopropylsilane. The peptide was then precipitated with 10 volumes of cold diethyl ether, and the terminal Fmoc was deprotected by a 15-min incubation with 20% (*v*/v) piperidine in DMF followed by a precipitation in cold diethyl ether. The resulting crude product was purified via preparative reversed-phase high-performance liquid chromatography (1290, Agilent) as described above. Finally, the purified targeting ligand was conjugated with different payloads via maleimide coupling also as described above.

2.4. Synthesis of mono-bisphosphonate targeting ligands

Alendronic acid was dissolved in sodium hydroxide and then diluted in MES buffer, and the pH was reduced to 5 with HCl. Three equivalents of 3-maleimidopropionic acid was pre-activated with 4 equivalents of EDC. The reaction was stirred overnight at 40 °C and the crude product was purified by preparative reversed-phase high-performance liquid chromatography (1290, Agilent)on a C-18 column using a 0–25% ammonium acetate/acetonitrile mobile phase for 40 min. The fractions that contained only pure maleimide product as analyzed by analytical liquid chromatography–mass spectrometry (1220 LC, 6130 MS, Agilent) were lyophilized and stored at −20 °C until required for coupling with payloads via maleimide coupling as described above.

2.5. Synthesis of tribisphosphonate targeting ligands

Di-tert-butyl-2,2′-((3-amino-2-(2-(2-(tert-butoxy)-2-oxoethoxy) ethyl)pentane-1,5-diyl)bis(oxy))diacetate was reacted with 1.5 equivalents of 3-maleimidopropionic acid, 4 equivalents of DCC, and 3 equivalents of DIPEA in DCM at 45 °C for 24 h. The DCU precipitate was filtered out and the volume reduced under low pressure. The product was purified via flash chromatography and the carboxylic acids were deprotected in 50:50 TFA/DCM for 30 min. The solvent was removed under reduced pressure and the resulting 2,2′-((2-(3-(carboxymethoxy)-1-(3-(2,5-dioxo-2,5-dihydro-1H-pyrrol-1-yl)propanamido)propyl) butane-1,4-diyl)bis(oxy))diacetic acid was reacted with 12 equivalents of alendronic acid plus 12 equivalents of EDC in MES buffer at pH 4.5 for 24 h at 45 °C. The resulting crude product was purified via preparative reversed-phase high-performance liquid chromatography (1290, Agilent) and the purified targeting ligand was conjugated with different payloads via maleimide coupling as described above.

2.6. Synthesis of polyphosphate targeting ligands

A phosphate glass polymer of 45 phosphates was dissolved in 100 mM MES at a concentration of 10 mM. Sufficient EDC was then added to achieve 100 mM concentration, and then 3 equivalents of DIPEA followed by five equivalents of N-(2-Aminoethyl)maleimide were added. The purified targeting ligand was conjugated with different payloads via maleimide coupling as described above.

2.7. Synthesis of 99mTc chelator molecules

^{99m}Tc chelators linked to D-Glu_{20} and D-Glu_{10} were synthesized via standard Fmoc solid-phase peptide synthesis as described previously. Wang resin loaded with Fmoc cysteine (TRT) was coupled to Fmoc aspartic acid (OtBu) then to N^{α}-Boc-N^{β}-Fmoc-*L*-2,3-diaminopropionic acid to create the ^{99m}Tc chelator [63]. This chelator was then coupled via standard amide chemistry to 8-(Fmoc-amino)-3,6-dioxaoctanoic acid, which was then conjugated via standard amide coupling to a linear oligopeptide of either 10 or 20 D-glutamic acids. The oligopeptide was then cleaved and purified as described previously.

2.8. Synthesis of NIR dye conjugates of bone fracture-targeting ligands

A maleimide derivative of the near infrared (NIR) fluorescent dye, S0456, was prepared for use in labeling of the bone fracture targeting ligands described above. It was synthesized as follows (see Fig. 1) For this purpose, S0456, N-Boc-tyramine and KOH were mixed in a flask containing DMSO to dissolve solids and the solution was stirred at 60 °C under argon for 1.2 h. The resulting solution was precipitated with cold ethyl acetate and, after vigorous agitation, was centrifuged at 3000 rpm for 3 min. The dark green solid was dried in a vacuum desiccator overnight and deprotected in 40% TFA/DCM for 30 min before being concentrated in vacuo to remove all TFA and DCM. The crude solid was then dissolved in water and subjected to preparative reversed-phase high-performance liquid chromatography (1290, Agilent) purification. Pure fractions were concentrated in vacuo and lyophilized. To derivatize with maleimide, the solid was dissolved in DMSO together with N-succinimidyl 3-maleimidopropionate and DIPEA and stirred under argon atmosphere for one hour before purification via preparative reversed-phase high-performance liquid chromatography (1290, Agilent) as described above. (L and D) Deca-aspartic acid-targeting ligand with an N terminal cysteine were prepared and purified as described previously. For conjugation of deca-aspartic acid cysteine to S0456-maleimide, S0456-maleimide was dissolved in DMSO in a flask degassed with argon, followed by the addition of Asp_{10}-cys to the solution with stirring. The mixture was stirred at room temperature for 2.5 h before purification with preparative reversed-phase high-performance liquid chromatography (1290, Agilent). The purified and lyophilized product appeared as a green fluffy solid. Synthesis of (D)Asp_{10}-S0456 conjugate followed the same procedure as described for (L)Asp_{10}-S0456, except that D-aspartic acid was used for the synthesis of (D)Asp_{10}.

2.9. Midshaft Femur fracture model

Aseptic surgical techniques were used to insert a 23-gage needle as an intramedullary nail into the femur of anesthetized 12-week-old female ND-4 Swiss-Webster age-matched mice for internal fixation on the bone prior to its fracture. No difference in targeting capacity was seen between inbred strains such as C57/BL6 and Swiss-Webster ND-4 mice (see supplemental Fig. 22). Briefly, the mouse hair surrounding the right knee of the hind paw was removed and the animal was anesthetized using 3% isoflurane with an anesthesia vaporizer(VetEqip). The skin was then cleaned with a scrub of betadine followed by a scrub of 70% ethanol. An incision was then made over the patella exposing the patellar tendon and the tendon was transected to expose the distal condyles of the femur. A sterile 23-gage needle was drilled through the cortical shell of the center of the patellar surface at the distal femur between the condyles and the pin was inserted down the center of the medullary cavity until it reached the endosteal surface of the proximal epiphysis of the femur. The needle was then cut with wire cutters to render it flush with the distal end of the femur and the skin was closed with 4–0 nonabsorbable nylon sutures. Fractures were then induced in the stabilized femurs using a drop-weight fracture device from RISystem and were verified via X-ray using an X-ray cabinet (Carestream, Kodak). The mice received buprenorphine (0.03 mg/day) for 3 days post-fracture to reduce pain. All animal experiments were performed in accordance with protocols approved by Purdue University's Institutional Animal Care and Use Committee (IACUC).

2.10. Analysis of the half-life and biodistribution of fracture-targeted fluorescent conjugates

To analyze the half-life of the targeted fluorescent conjugates at the fracture site, L-Asp_{10}-S0456 or DAsp_{10}-S0456 were dissolved in PBS, sterile filtered, and injected 10 days (see supplemental Fig. 16) post-

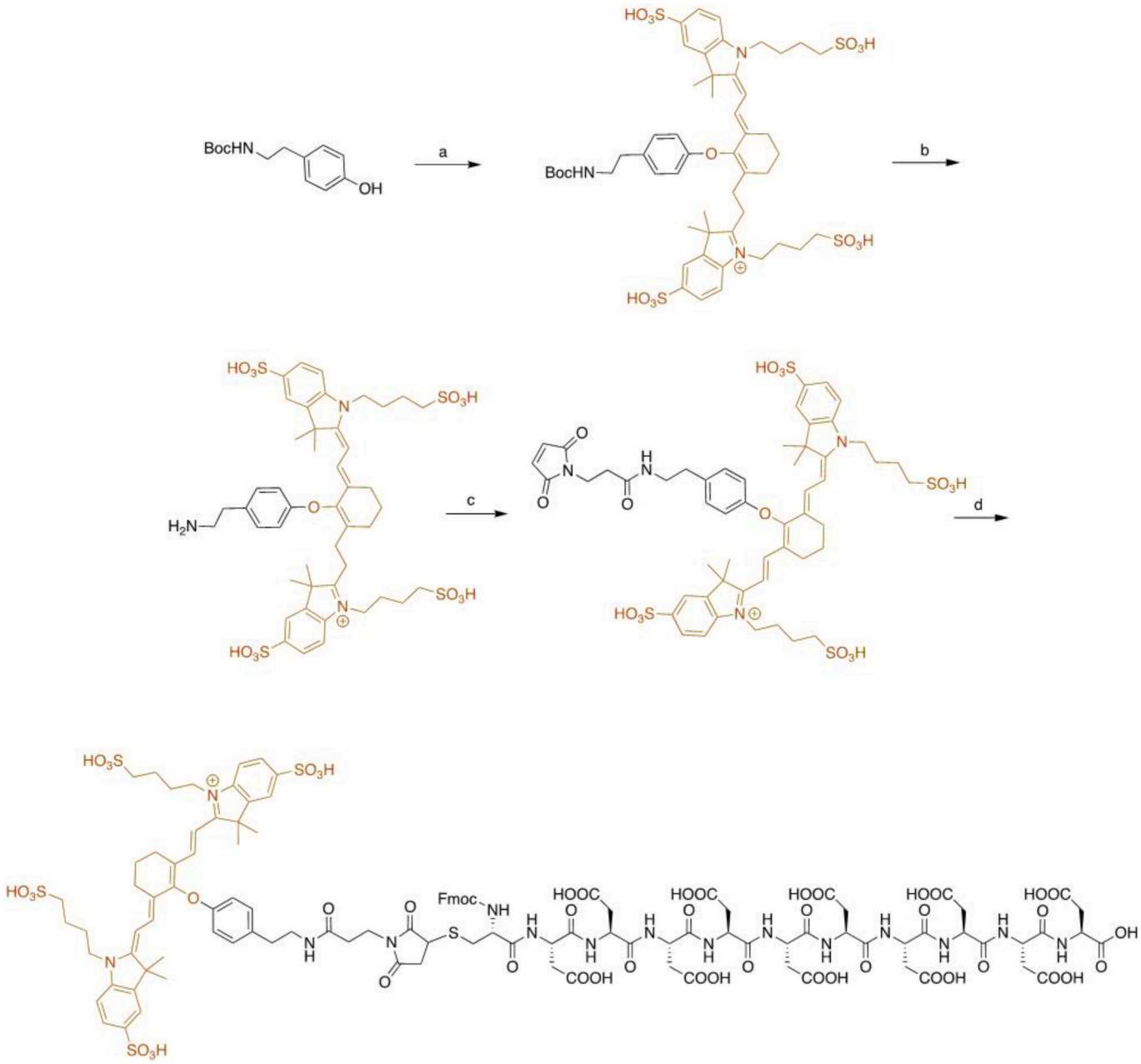

Fig. 1. Synthesis of (L)Asp$_{10}$-S0456 conjugate. Reagents and conditions: A) S0456—Cl, DIPEA, DMSO, 60 °C B) 40% TFA/DCM, rt. C) N-succinimidyl 3-maleimido-propionate, DIPEA, DMSO, rt. D) Asp$_{10}$-cys, DMSO.

fracture subcutaneously to achieve a final dose of 250 nmol/mouse. Mice were then euthanized at 2, 24, 48, 72, and 96 h post-injection and fluorescence was quantified at the fracture site by resecting the and dissolving the fracture callus in a 12% solution of neutral buffered EDTA. Briefly, broken femurs were collected, rinsed with PBS, dried thoroughly overnight in a vacuum desiccator, broken into small pieces, and weighed before immersing in the aforementioned EDTA solution. The sample was agitated on a shaker for 8 h to decalcify the bone and then centrifuged for 5 min at 8000 rpm to collect the supernatant. The concentration of L-Asp$_{10}$-S0456 or DAsp$_{10}$-S0456 in the supernatant was then determined from its OD780 using a standard curve of known concentrations of the dye for quantitation.

2.11. Radiolabeling of peptides with ^{125}I or ^{99m}Tc

10 μg of Pierce Iodination (iodogen) reagent was dissolved in 200 μL chloroform, then added to a 6 × 50 mm glass test tube and evaporated under a steady stream of argon. Then 50 nmol of peptide conjugate dissolved in 40 μL of PBS was added together with 10 μL(1 mCi) of Na^{125}I(ARC). The glass test tubes were sealed and placed on a shaker for 30 min and then purified via radio preparative reversed-phase high-performance liquid chromatography (1260 HPLC, Agilent Flow-RAM radiodectector, Lablogic) with a 0–100% gradient of 0.1% TFA in water:acetonitrile. Fractions with the correct retention time and radio signal were isolated and lyophilized. Payload peptides were radio-iodinated on endogenous tyrosine, tryptophan, or histidine residues, which remain stable in physiological conditions for the longest iodinated experiments (27 h) [64].

For ^{99m}Tc labeling, 0.6 mg of EDTA disodium dihydrate dissolved in nitrogen-sparged water (10 mg/ml) was added to 50 mg of sodium gluconate solution (100 mg/ml) in nitrogen-sparged water. To that mixture, a solution of 0.2 mg of tin chloride dihydrate (10 mg/ml)

dissolved in nitrogen-sparged 0.2 N HCl was added. Then 4 μmol of ^{99m}Tc chelate-containing peptides were added to the solution and the pH was adjusted to 6.8 using NaOH [63]. The solution was flash frozen in liquid nitrogen and lyophilized overnight. The compound was then mixed with 15 mCi of m^{99}Tc (Cardinal Health) and after 15 min of shaking, quantitative chelation was confirmed by analytical radio reversed-phase high-performance liquid chromatography (1260 HPLC; Agilent Flow-RAM radiodectector, Lablogic).

Biodistribution Analyses of Radiolabeled PeptidesFor live animal studies, ^{99m}Tc- or ^{125}I-radiolabeled peptides were dissolved in PBS and injected subcutaneously into mice 10 days after induction of a midshaft femur fracture to ensure that blood flow had returned to the area. Each mouse received a 0.25 mCi (12.5 nmol of peptide in 0.1 mL vehicle) dose of radio-iodinated peptide or 3 mCi (0.1 ml) dose of ^{99m}Tc-labeled peptide, both administered subcutaneously. Eighteen hours later, (see supplemental figs. 14 and 15), blood was removed via cardiac puncture, and mice were sacrificed via CO_2 asphyxiation. Organs and tissues (heart, lungs, muscle, skin, liver, spleen, kidneys, fractured femur, and healthy femur) were resected and weighed, and their radioactivity was counted using a gamma counter (Cobra Auto-Gamma, Packard). Percent injected dose was calculated by:

$$\%injected\ dose = \frac{Tissue(counts)}{Injection\ (counts) \times Tissue(grams)} \times 100$$

Fractured to healthy ratio was calculated by:

$$Fractured\ to\ healthy\ ratio = \frac{The\ fractured\ femur's\%injected\ dose}{The\ healthy\ femur's\%injected\ dose}$$

2.12. SPECT/CT

^{99m}Tc labeled D-Glu$_{10}$-chelator and D-Glu$_{20}$-chelator were formulated to 7 mCi/100ul and injected via tail vein two weeks following femur fracture. After 18 h, mice were euthanized via CO_2 asphyxiation and imaged using a SPEC/CT scanner (U-SPECT-II/CT, MiLabs). CT images were collected using high resolution full body 12-min scans and were followed by 1-h SPECT scans using a 0.6 mm collimator. SPECT images were reconstructed using the MiLabs software selecting the energy window of 140 keV and reconstruction parameters of 16 subsets and 4 iterations without post filter. 3D reconstructions were performed using ImageJ software.

2.13. Statistics

All statistical analyses were performed with GraphPad Prism (version 8.0; GraphPad Software, CA). Data are displayed as mean ± standard deviation. In the figures, levels of statistical significance are denoted with asterisks according to the following definition: $*p < 0.05$; $**p < 0.01$; $***p < 0.001$; $****p < 0.0001$. Statistical analysis was performed using a one-way analysis of variance (ANOVA) and a Dunnett's post-hoc analysis with adjusted significance reported at the P value of 0.05. For Figs. 4-8 a Bonferroni post-hoc analysis was performed instead of a Dunnet's post-hoc analysis. Fig. 9 was analysied with a Two way ANOVA with a Dunnett's post hoc analysis.

3. Results

As mentioned previously, a variety of low-molecular-weight ligands have been found to exhibit a tropism for the hydroxyapatite that is exposed in osteoporotic bone, malignant bone lesions, and fracture surfaces. Because the same targeting molecules have been used to deliver imaging agents to these lesions, we undertook to determine whether similar ligands might be exploited to deliver anabolic drugs to fracture sites, thereby enabling repeated dosing of bone anabolic agents over the entire course of the fracture healing process. For this purpose, each of the above ligands along with additional targeting molecules described below was linked via standard coupling chemistries to either imaging agents or bone anabolic peptides and examined for their specificities for fracture surfaces in mice containing midshaft femur fractures. As shown in Fig. 2, when each of the previously-characterized hydroxyapatite targeting ligands [48,60] (panel A) was labeled with ^{125}I-tyrosine and injected intravenously into fracture-bearing mice, the targeting ligands accumulated with different specificities at the femur fracture site (panel B). Whereas the ratio of ^{125}I-labeled tetracycline in the fractured to healthy femur was only 2.6 This could be due in part to iodination of tetracycline itself, however, compared to tyrosine, the iodination of tetracycline is inefficient [65] and the site of iodination is ortho/para from the C10 carbon and is unikely to interfere with binding [40,66]. The fractured-to-healthy ratio was continuously increased as the tetracycline ligand was exchanged for alendronate, polyphosphate, and an acidic octa-aspartic acid. Taken together, these data suggest that the octa-aspartic acid may possess the highest specificity for fractured over healthy bone with a selectivity ratio of 11.2, while tetracycline likely displays the lowest. Based on this ranking and the fact that tetracyclines are also encumbered by serious toxicities [67,68], we elected to dismiss tetracyclines from further consideration for fracture-targeted drug delivery as they were 4.2 times less selective than octaaspartic acid.

Although bisphosphonates and polyphosphates were also found to exhibit reduced specificity for fractured bone, we still decided to include them in a comparison of peptide targeting abilities, since most bone anabolic agents are peptides or proteins [69–73]. For this purpose, the N-terminal 34 amino acids of parathyroid hormone-related protein (PTHrP), a peptide frequently used to stimulate bone formation [74], was labeled with ^{125}I and tethered to a monobisphosphonate (alendronate), a tribisphosphonate comprised of three alendronates attached to a central hub (Supplemental Fig. 26), a polyphosphate consisting of 45 phosphates connected by anhydride linkages [75,76], or a deca-aspartic acid similar to the octa-aspartic acid examined above. As shown in Fig. 3, use of the monobisphosphonate (alendronate) as the targeting ligand enabled delivery of a moderate amount of ^{125}I-PTHrP (1–34) to the fracture site, also displaying reasonable specificity of 2:1 for broken bone over healthy bone (see Fig. 3, panel C). However, use of the more complex ligand comprised of 3 alendronates surprisingly resulted in diminished rather than enhanced fracture targeting. And, as seen in Fig. 3, the polyphosphate again provided minimal ^{125}I-PTHrP (1–34) delivery to the fracture surface with only 1.55% of injected drug being present on the fracture surface 24 h later, while an acidic oligopeptide (AOP) comprised of 10 aspartic acids yielded the highest specific delivery to the fractured bone with 3.5 times more specificity for the fracture and accumulation in the fracture than monobisphosphonates (see Fig. 3, panel B). Based on these data and the unwanted inhibitory activities [77] of bisphosphonates on osteoclasts, we decided to focus all further targeting studies on variations in the structures of acidic oligopeptides. In this effort, five variables were envisioned to potentially impact the ability of an AOP to deliver an attached anabolic peptide to a fracture surface: (1) chemical characteristics of payload, (2) AOP side chain structure, (3) AOP length, (4) AOP branching, and (5) AOP stability). We elected to address each of these variables sequentially in the paragraphs below.

3.1. Effect of payload characteristics on fracture targeting with acidic oligopeptides

To explore the impact of the therapeutic payload's composition on the ability of an attached AOP to concentrate the active drug at a fracture site, we compared the abilities of AOPs to deliver a variety of bone anabolic peptide cargoes of carefully selected properties, including 1) size, 2) charge, and 3) hydrophobicity. First, to compare anabolic peptides of different charge, we selected CK2.3 [78] as a representative cationic peptide with a net charge of +5, ODP [79] as a representative anionic peptide with a net charge of −3, and CTC [80,81] as a representative neutral peptide with a net charge of 0. P4 [10,82] was also

A.

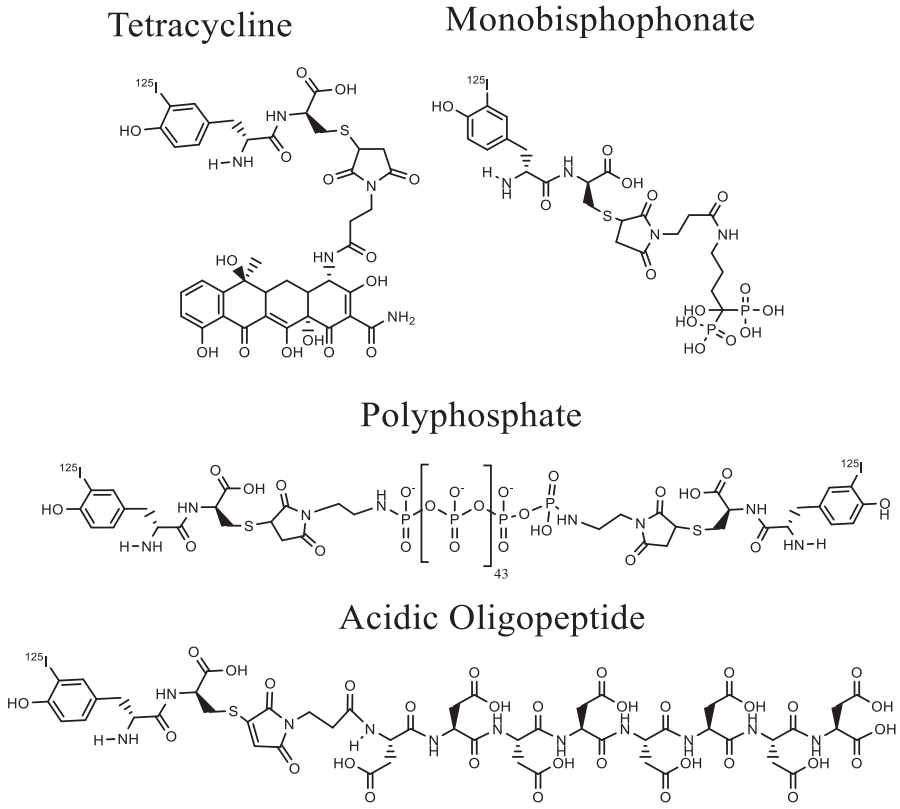

B.

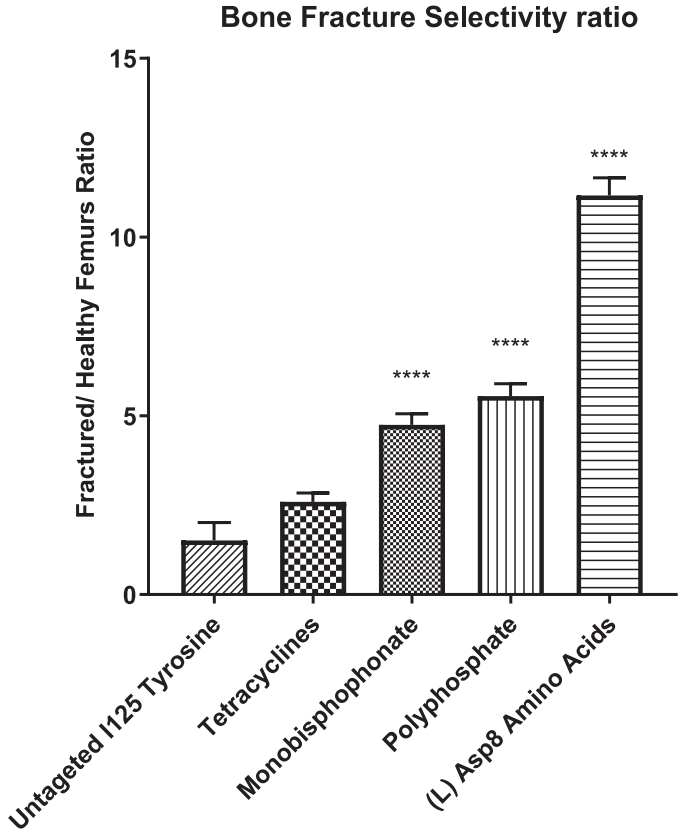

Fig. 2. Comparison of selectivity for the fracture selectivity over the rest of the skeleton. A) The structures of tetracycline, monobisphosphonate,polyphosphate, and acidic oligopeptide targeting ligands conjugated to a radiolabeled tyrosylcysteine via a maleimide coupling. B) The ratio between the accumulation in the fracture callus and in the contralateral healthy femur for the established bone-targeting ligands delivering ^{125}I tyrosylcysteine payloads (see panel A). Levels of statistical significance are denoted with asterisks according to the following definition: $*p < 0.05$; $**p < 0.01$; $***p < 0.001$; $****p < 0.0001$.

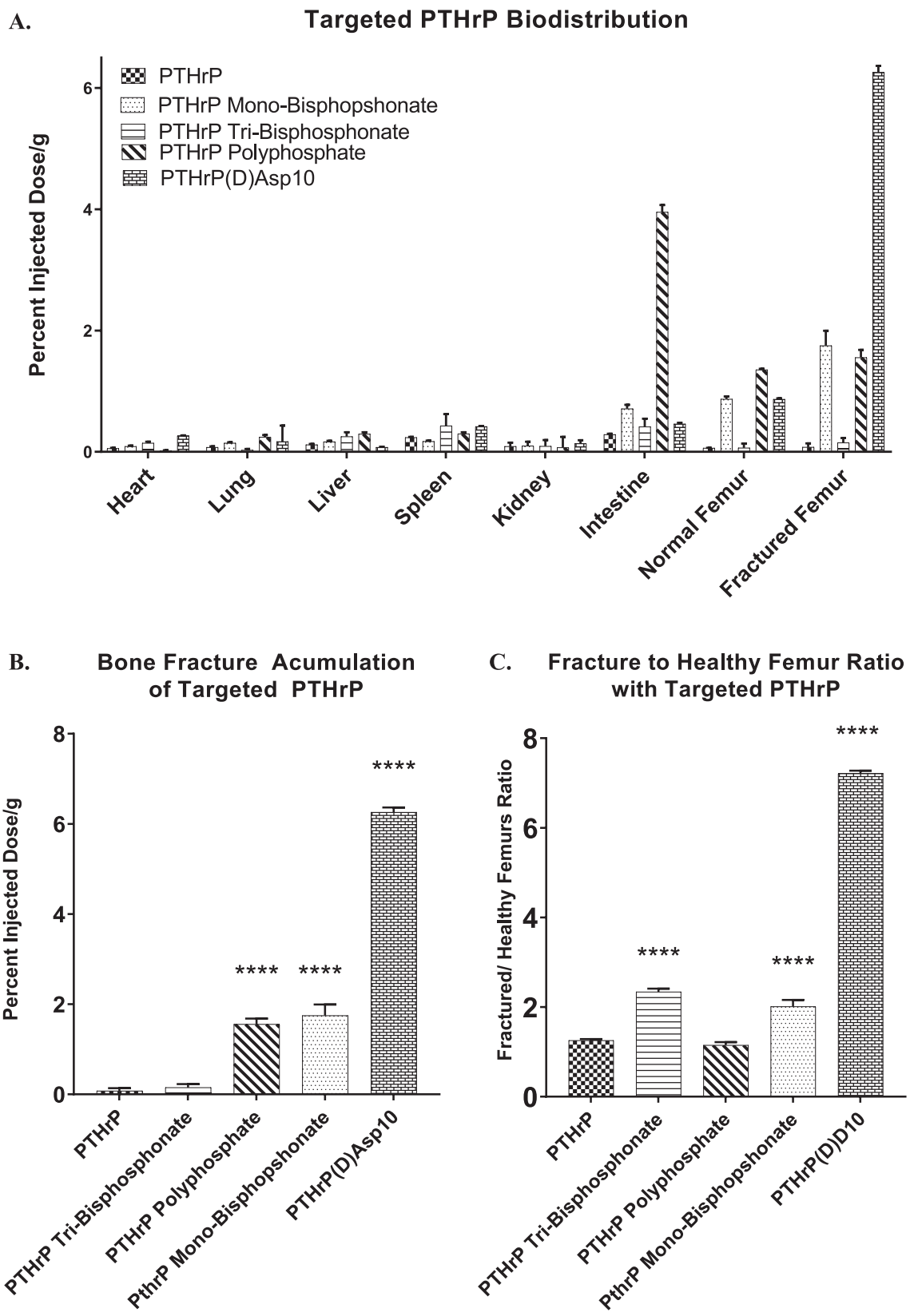

Fig. 3. The biodistribution of radio-iodinated PTHrP coupled to different hydroxyapatite -binding moieties 24 h post-injection. A) The accumulation of the labeled compounds in different tissues are reported as a percent of the injected dose. B) Accumulation of targeted and free PTHrP in the fractured femurs of mice 24 h post-injection. C) The selectivity ratio between the fracture callus and the contralateral healthy femur. D). Levels of statistical significance in panels B and C are denoted with asterisks according to the following definition: $*p < 0.05$; $**p < 0.01$; $***p < 0.001$; $****p < 0.0001$.

included as a representative of a hydrophobic peptide with a hydrophobicity index (GRAVY) of 0.49. Finally, to assess the impact of cargo size, F109 [83,84], PACAP [85], and CK2.3 were also included, because F109 has a chain length of only 9 amino acids while the latter two have chain lengths of 39 and 30 amino acids, respectively (Table 1). All of the above bone anabolic peptides were linked to L-Asp_{10}, radiolabeled with iodogen ^{125}I, injected into mice with fractured femurs, and allowed to circulate for 18 h before evaluation for tissue biodistribution [85].

As shown in Fig. 4, the chemical properties of the various peptides exerted little impact on the ability of L-Asp_{10} to target them to fracture surfaces. In fact, only the 39 amino acid PACAP differed somewhat from the other anabolic peptides in fracture targetability. However, because a peptide of similar length (CK2.3) displayed no reduction in fracture accumulation, we conclude that neither payload size nor any other major chemical/physical variable exerts a consistent impact on AOP-mediated bone targeting. Indeed, the fact that all other anabolic cargoes seem to target similarly would suggest that an attached AOP should dominate the biodistribution of most peptidic cargoes.

3.2. Effect of acidic oligopeptide branching on fracture targeting

To explore the impact of peptide branching on payload targeting, we compared the abilities of acidic oligo-aspartic acids constructed of either two chains of 5 aspartic acids each or a single linear chain of 10 aspartic acids to deliver the Ck2.3 payload to fracture surfaces. As seen in Fig. 5, linear peptides were found to concentrate 2.7 times better on fracture surfaces than branched peptides. Moreover, since nontargeted Ck2.3 displayed little uptake at the fracture site, nonspecific trauma-mediated deposition of Ck2.3 could be dismissed as a major contributor to the accumulation of the acidic oligopeptide conjugate at the fracture site.

3.3. Effect of acidic oligopeptide side chain length on fracture targeting

Assuming that the interaction of AOPs with a bone fracture surface is primarily mediated by its interaction with exposed calcium, molecular orbital studies would dictate that calcium should chelate best when the proximal anionic charges are separated by a distance of 8.6A [86]. Recognizing that the lengths of the anionic side chains of our AOPs would determine this separation distance between negative charges, we elected to compare the targeting abilities aspartic acid, glutamic acid

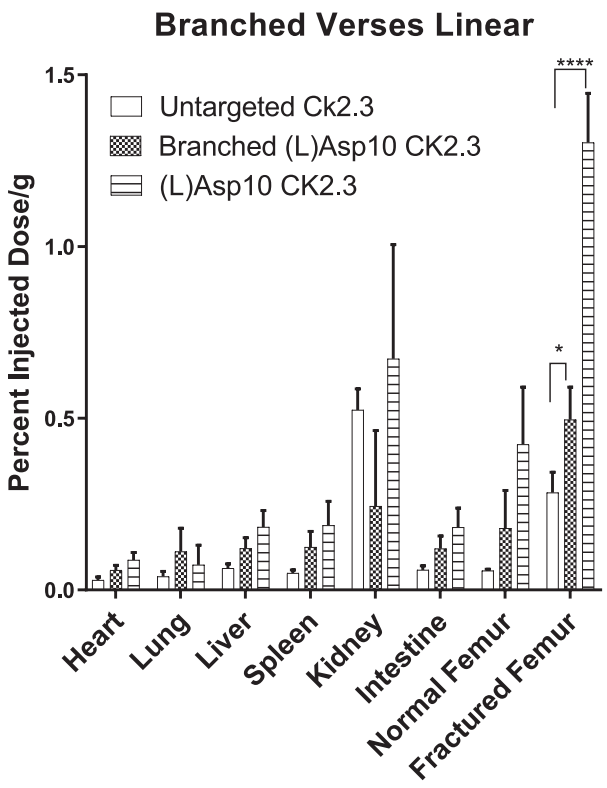

Fig. 5. The biodistribution of radio-iodinated CK2.3 coupled to branched or linear chains of 10 (L) aspartic acids relative to untargeted CK2.3. The biodistributions were determined 18 h post-injection into ND-4 Swiss-Webster mice ($n = 5$) bearing midshaft femur fractures 10 days post-fracture. The accumulation of the labeled compounds in different tissues are reported as a percent of the injected dose per gram of tissue. Levels of statistical significance are denoted with asterisks according to the following definition: $^{*}p < 0.05$; $^{**}p < 0.01$; $^{***}p < 0.001$; $^{****}p < 0.0001$.

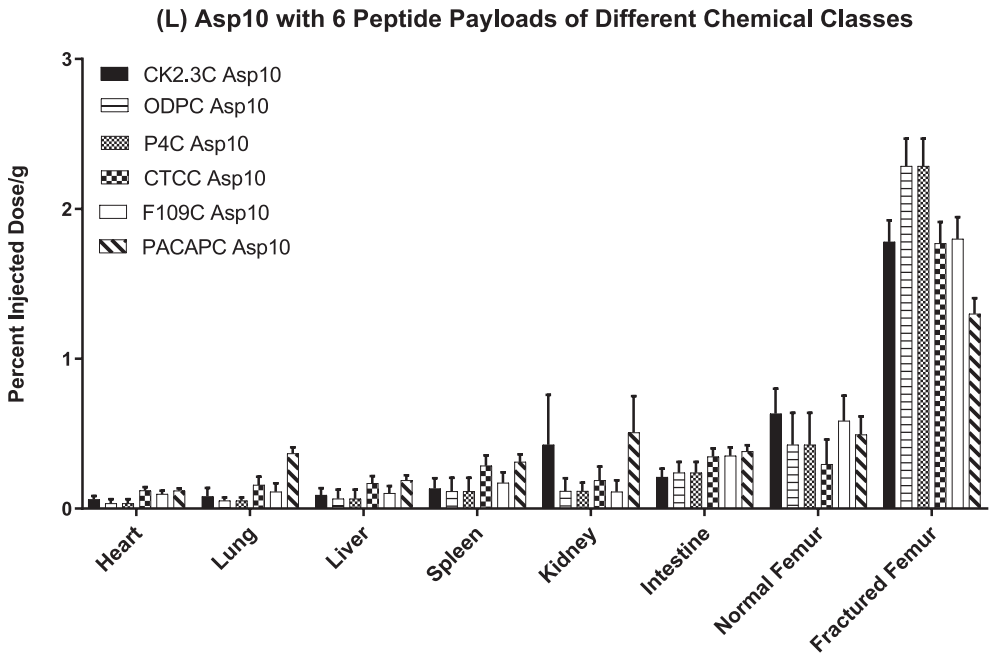

Fig. 4. The biodistribution of six different radio-iodinated payloads coupled to (L) Asp_{10} 24 h post-injection into ND-4 Swiss-Webster mice ($n = 6$) bearing midshaft femur fractures 10 days post-fracture. The selected peptide payloads are representative of different chemical classes (see Table 1). The accumulation of the labeled compounds in different tissues are reported as a percent of the injected dose per gram of tissue. Levels of statistical significance are denoted with asterisks according to the following definition: $^{*}p < 0.05$; $^{**}p < 0.01$; $^{***}p < 0.001$; $^{****}p < 0.0001$.

and aminoadipic acid, where the side-chain carboxyls extend from the peptide backbone by one, two, and three carbons, respectively, allowing an increasing separation between the anionic charges of the oligopeptide side chains.

As seen in Fig. 6, decaglutamic and deca-aspartic acids exhibited the greatest uptake at the fracture site with 6 times more accumulation than the nontargeted Ck2.3, and with aminoadipic acid promoting bone fracture retention not significantly different from nontargeted Ck2.3. These data demonstrate that an AOP comprised of either glutamic or aspartic acids constitutes a peptide with optimal charge separation for calcium binding and may help explain the branched peptide's reduction in binding. The fact that nature has primarily selected glutamic acids for its calcium binding functions in bone mineralization [87], together with the repeated observation that the synthesis of glutamic acid oligomers is much more efficient than aspartic acid oligomers due to unwanted formation of aspartamides, [88,89] prompted us to focus all further bone fracture-targeting efforts on the optimization of the glutamic acid oligomers.

3.4. Effect of linear Oligoglutamic acid length on fracture targeting

To explore the impact of oligopeptide length on fracture-targeting ability, we compared the abilities of oligoglutamic acids of 10 or 20 amino acid lengths to deliver the same CK2.3 cargo to fractured femur surfaces. As seen in Fig. 7, CK2.3 tethered to the longer oligoglutamic acid accumulated 3.3 times more at the fracture site than the shorter oligoglutamic acid. While the affinities of unconjugated acidic oligopeptides seem to maximize at chain lengths of only 8 amino acids [44], the observed increased affinity of the 20-mer over 10-mer probably arises because more extensive binding to hydroxyapatite is required to retain a payload of the size of CK2.3 at the fracture surface. The improved localization of the CK2.3 payload with the 20-mer could also be in part due to a relative reduction in steric hinderance from the payload on the targeting ligand.

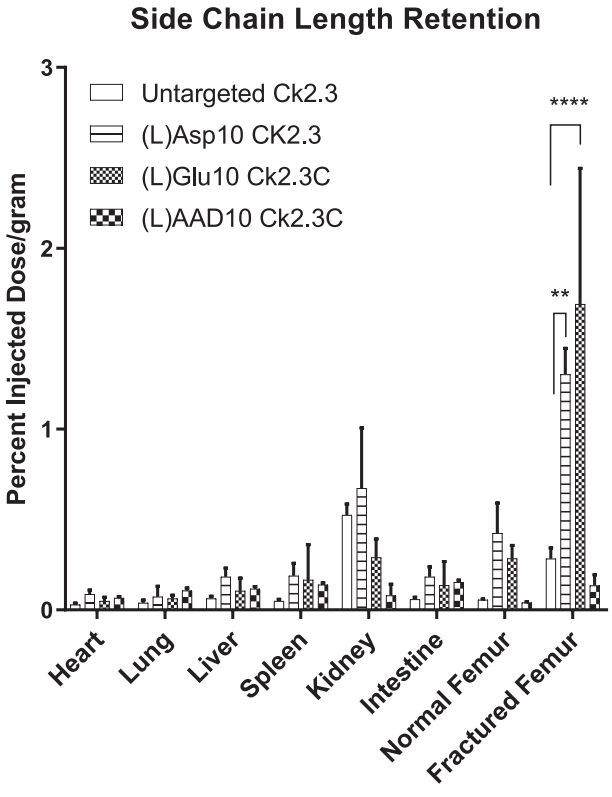

Fig. 6. The biodistribution of radio-iodinated CK2.3 coupled to linear chains of 10 (L) aspartic acids, 10 (L) glutamic acids, or 10 (L) aminoadipic acids relative to untargeted CK2.3. The biodistributions were determined 18 h post-injection into ND-4 Swiss-Webster mice ($n = 5$) bearing midshaft femur fractures 10 days post-fracture. The accumulation of the labeled compounds in different tissues are reported as a percent of the injected dose per gram of tissue. Levels of statistical significance are denoted with asterisks according to the following definition: $^{*}p < 0.05$; $^{**}p < 0.01$; $^{***}p < 0.001$; $^{****}p < 0.0001$.

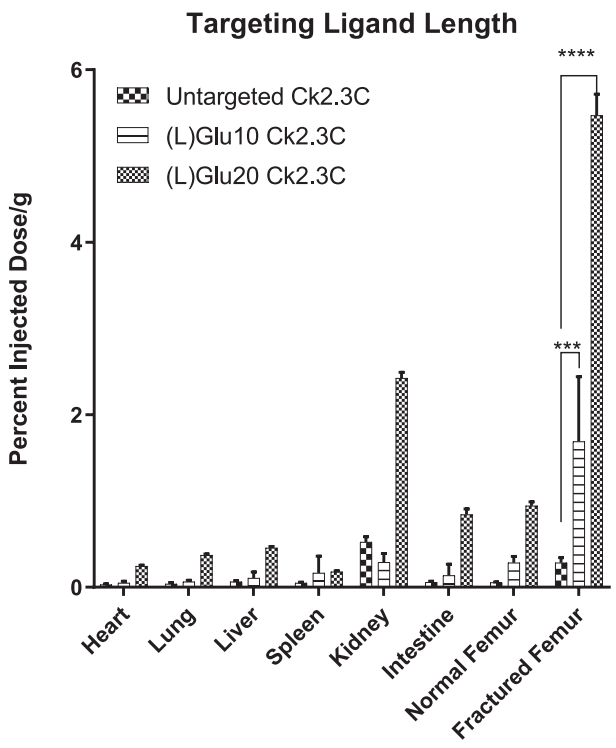

Fig. 7. The biodistribution of radio-iodinated CK2.3 coupled to linear chains of 10 or 20 (L) Glutamic acids relative to untargeted CK2.3. The biodistributions were determined 18 h post-injection into ND-4 Swiss-Webster mice ($n = 5$) bearing midshaft femur fractures 10 days post-fracture. The accumulation of the labeled compounds in different tissues are reported as a percent of the injected dose per gram of tissue. Levels of statistical significance are denoted with asterisks according to the following definition: $^{*}p < 0.05$; $^{**}p < 0.01$; $^{***}p < 0.001$; $^{****}p < 0.0001$.

.

3.5. Effect of acidic oligopeptide stereochemistry on fracture targeting: comparison of d versus l oligoglutamic acid

Studies by other groups have demonstrated that acidic oligopeptides are not readily orally bioavailable [90], suggesting that the likely route of administration must be by injection. Unfortunately, drugs requiring frequent injection can discourage patient compliance, suggesting that a longer-lasting formulation that would require fewer injections might achieve greater adoption in the clinic[91,92]. Because the affinities of acidic oligopeptides comprised of D- and L-amino acids for hydroxyapatite have been found to be similar [44], we elected to explore whether a linear oligoglutamate chain composed of poorly-metabolizable D-glutamic acids rather than a readily-digestible chain comprised of L-glutamic acids might lead to longer drug retention at the fracture surface. To test this hypothesis, we compared the abilities of the D and L enantiomers of glutamic acid 20-mers to accumulate and persist at the fracture site. As shown in Fig. 8, we found that the D enantiomer of Glu_{20} accumulated 4.7 times more than the L enantiomer at the fractured femur and 91.9 times as much as the nontargeted Ck2.3. To further investigate the impact of this stereochemistry on retention half-life and to see if this impact existed for the more-established shorter aspartic acid polymers as well, we attached the fluorescent dye, SO456, to both D an L

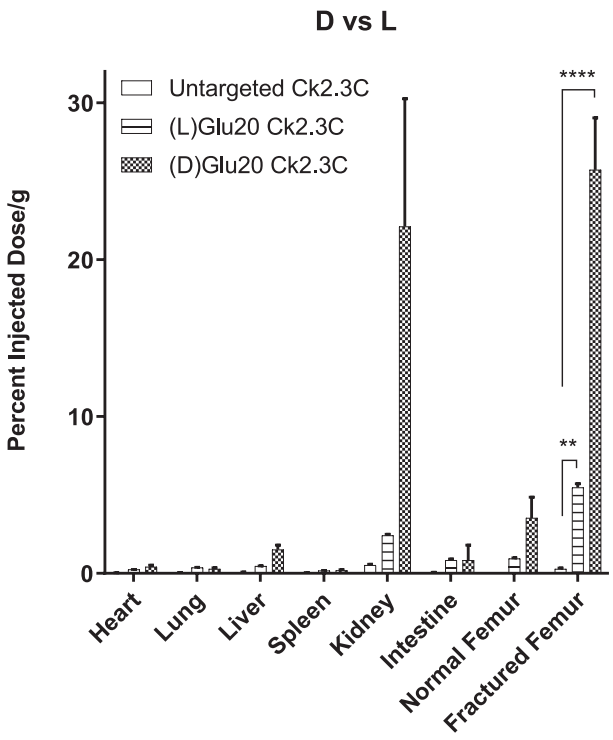

Fig. 8. The biodistribution of radio-iodinated CK2.3 coupled to linear chains of 20 L- or D-glutamic acids relative to untargeted CK2.3. The biodistributions were determined 18 h post-injection into ND-4 Swiss-Webster mice ($n = 5$) bearing midshaft femur fractures 10 days post-fracture. The accumulation of the labeled compounds in different tissues are reported as a percent of the injected dose per gram of tissue. Levels of statistical significance are denoted with asterisks according to the following definition: $^{*}p < 0.05$; $^{**}p < 0.01$; $^{***}p < 0.001$; $^{****}p < 0.0001$.

enantiomers of Asp_{10} peptides (see Fig. 1) and quantified the accumulation of the differently-labeled enantiomeric chains in both fractured and healthy contralateral femurs. As shown in Fig. 9, the L enantiomer exhibited a half-life of ~ 35 h, whereas the D enantiomer displayed a half-life nearly 3 times as long of ~ 100 h. The difference was slight smaller than that detected with radiolabled peptide payloads. This is likely due to the shorter half-life of the peptide payloads relative to the fluorescent payload. Curiously, this same enhanced stability resulted in prolonged clearance through the kidneys, probably because the slowly degradable D-isomer released more slowly from the bone and other tissues than the L-isomer. More importantly, D-Glu_{20} was demonstrated to deliver significantly more cargo to the fracture site than any of the other targeting ligands (see Fig. 10).

3.6. *Comparison of fracture localization of D-Glu_{10} and D-Glu_{20} oligopeptides*

Finally, to visually compare the biodistributions of the D-Glu_{10} and D-Glu_{20} oligopeptides, since the impact of extending the targeting ligand was greater than expected, we performed SPECT/CT imaging of both oligopeptides and examined their biodistributions visually. As shown in Fig. 11A, both acidic oligopeptides yielded highly resolved images with the targeted radio-imaging agents almost exclusively concentrated at the fracture site. Signal to volume ratios are greater than 10-fold higher in the fracture than in other adsorption sites such as the growth plates. Still, the adsorption to the growth plates may limit patients to adults. Because of the similarity between the two images, a second biodistribution analysis was conducted (panel C) with results very similar to those in Fig. 10; i.e. D-Glu_{20} accumulating ~ 5 times more efficiently at the fracture site than D-Glu_{10}. Due to its high avidity and lower steric hinderance, D-Glu_{20} exhibits the greatest fracture-targeting capacity of all ligands tested, and assuming that the radioactivity observed in the kidneys constitutes unbound drug still undergoing excretion, the D-Glu_{20} oligopeptide probably also displays the greatest selectivity for fracture sites of all targeting ligands tested.

4. Discussion

Bone targeting has existed for over 30 years [93], during which time it has primarily focused on delivering payloads to orthopedic pathologies not related to fractures, such as osteoporosis [54], osteomyelitis [37], and bone metastases [52]. These treatments have primarily used bisphosphonates [94] to deliver compounds selectively to bone. However, when treating bone fractures, it is imperative to deliver compounds selectively to the fracture site to avoid ectopic ossification that can occur when drug is delivered nonspecifically to all bone. For that purpose, we

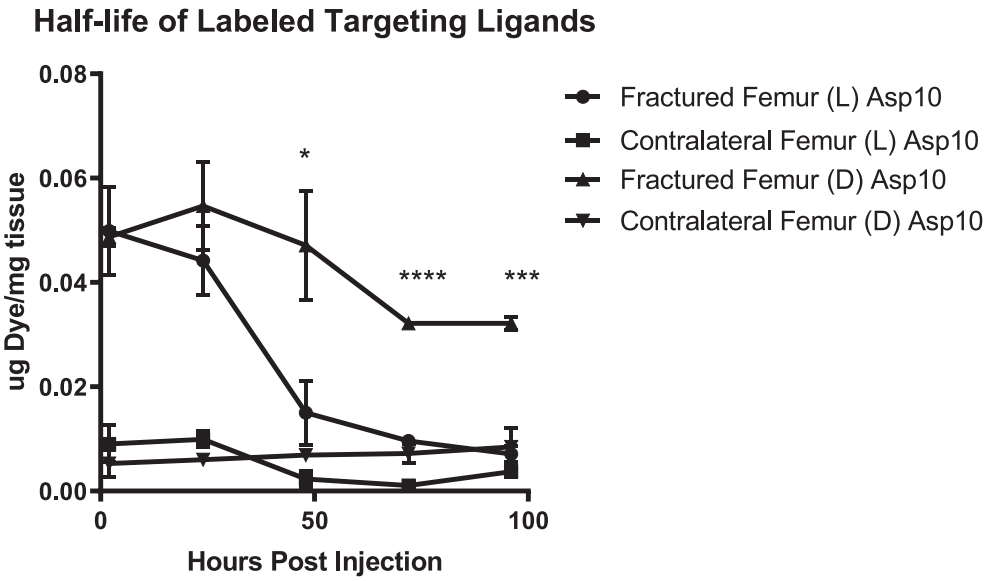

Fig. 9. The accumulation of S0456 (near-IR fluorophore) coupled to linear chains of 10 L- or D-aspartic acids in ND-4 Swiss-Webster mice bearing midshaft femur fractures 10 days post-fracture at different time points post-injection. The accumulation of the labeled compounds in the healthy (undamaged contralateral femur) and the broken femur are quantified as the amount of labeled dye that was extracted from dissolved femurs post-mortem. The retention half-life of Asp_{10} was estimated to be ~35 h, whereas that of (D)Asp_{10} was projected to be over 100 h. 250 nmol of compound were injected. ($n = 5$ for mice receiving L-Asp10, and $n = 3$ for mice receiving D-Asp10). Error bars represent standard error of mean. (see supplemental Figs. 24 and 25). Statistical significance is show for the difference between L and D enatomers accumulation in the fractured femur. Significance was calculated via a two way ANOVA. Levels of statistical significance are denoted with asterisks according to the following definition: $^{*}p < 0.05$; $^{**}p < 0.01$; $^{***}p < 0.001$; $^{****}p < 0.0001$.

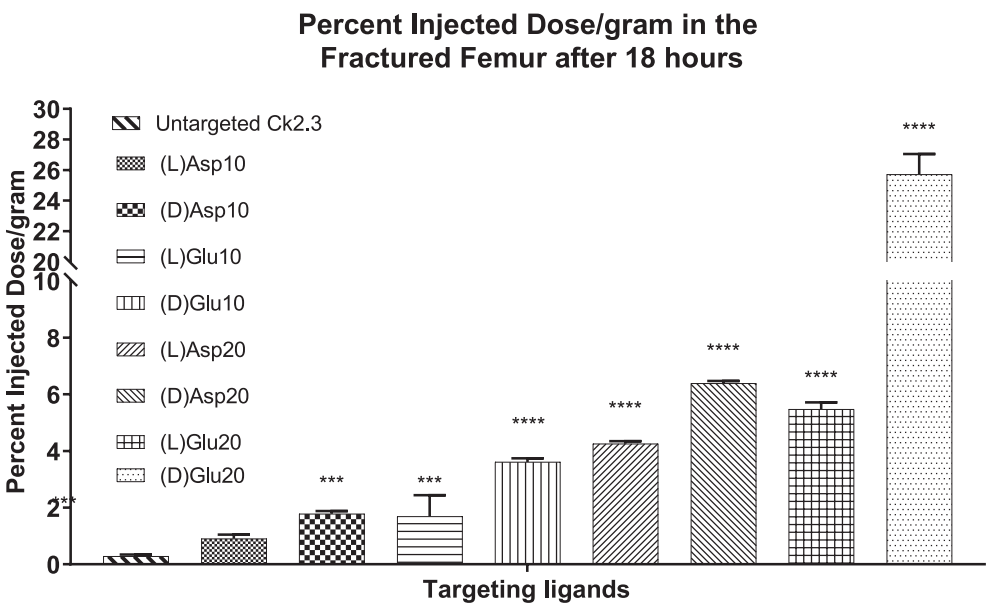

Fig. 10. The accumulation in fractured femurs of radio-iodinated CK2.3 coupled to different acidic oligopeptides relative to untargeted CK2.3. The biodistributions were determined 18 h post-injection into ND-4 Swiss-Webster mice (n = 5) bearing midshaft femur fractures 10 days post-fracture. The accumulation of the labeled compounds in the fractured femurs are reported as a percent of the injected dose per gram of tissue. Levels of statistical significance are denoted with asterisks according to the following definition: $*p < 0.05$; $**p < 0.01$; $***p < 0.001$; $****p < 0.0001$.

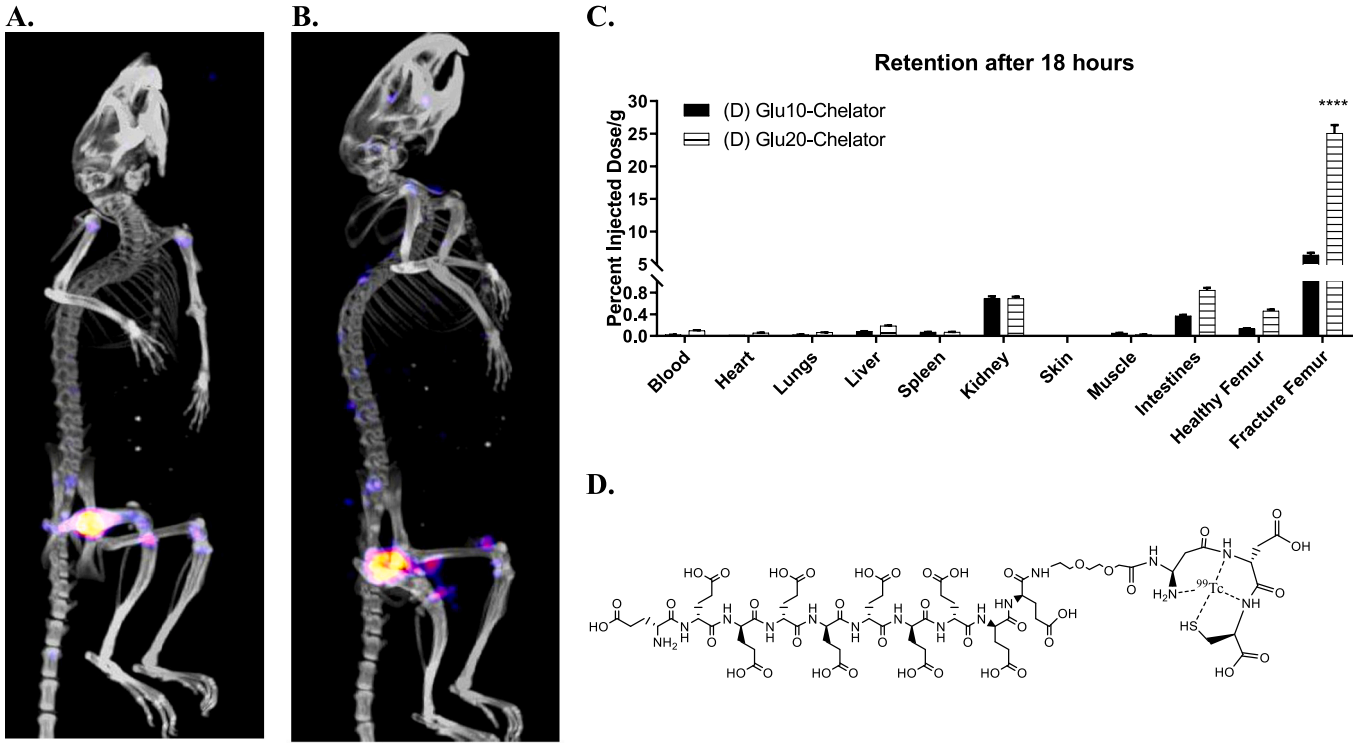

Fig. 11. Acidic oligopeptide labeled with 99Tc and imaged at 18 h post-injection using SPECT/CT in mice with midshaft femur fractures 10 days post-fracture. A) SPEC/CT image of the Tc chelator EC20 chelating 99Tc linked to $(D)Glu_{10}$ acid. B) SPEC/CT image of the Tc chelator EC20 chelating 99Tc linked to $(D)Glu_{20}$. C) The structure of EC20 $(D)Glu_{10}$ chelating 99Tc. D) The quantification of the accumulation of the labeled $(D)Glu_{10}$ and $(D)Glu_{20}$ compounds in the different tissues as a percent of injected dose per gram ($n = 10$). The majority of signal is observed in the fracture callus of the femur. Trace concentrations of drug can be observed at sites of high bone turnover. $(D)Glu_{10}$ and $(D)Glu_{20}$ have similar specificities, but $(D)Glu_{20}$ has a longer retention in the bone.

undertook to compare the fracture selectivities of the many bone targeting molecules already described in the literature.

When we compared all candidates, we were surprised to observe that tetracycline was only moderately selective for fractured over healthy bone [42]. Considered together with the fact that tetracyclines can be toxic to bone, liver and kidney [67] we concluded that potential problems with tetracyclines would far outweigh their benefits in fracture localization.

Several limitations also existed with using bisphosphonates for fracture targeting, including the fact that they inhibit osteoclasts which are essential for both normal skeletal remodeling and resolving of fracture calluses from woven bone into laminar bone. While work has been done to create bisphosphonates that do not inhibit osteoclasts [52], little is understood regarding the effects of their long-term use on the skeleton, since they act as mineralization inhibitors independently of their Farnesyl Pyrophosphate Synthetase inhibition (FFPS) [95].

Another problem with using bisphosphonates as targeting ligands is that they have half-lives of up to 20 years in bone [77], potentially leading to an undesirably prolonged stimulation of their molecular targets, depending on the stability of their therapeutic cargoes.Although bisphosphonates have still other worrisome toxicities (e.g. osteonecrosis of the jaw), their legacy as targeting ligands for bone led us to evaluate their performance as bone fracture targeting moieties. We found that bisphosphonates could semi-selectively deliver compounds to the fracture site, i.e. consistent with the biodistribution seen in an MDP bone scan [96]. They, however, were not effective at delivering large anabolic peptides to the fracture callus. It is likely that a bisphosphonate's smaller contact area relative to that of an acidic oligopeptide is responsible for this reduction in targeting capacity. While it was expected that a multivalent bisphosphonate should improve on the monovalent's targeting capacity, the tribisphosphonate performed surprisingly worse. This could be due to either incorrect spacing between the bisphosphonates or an inability of all bisphosphonates in the tribisphosphonate to interact maximally with the bone fracture surface. More recent work has uncovered a new targeting ligand pyrophosphate which is similar to the polyphosphate used in this paper which mimics bisphosphonates' targeting abilities but has a much shorter half-life like AOP's [97]. This could get around some of the half-life issues that bisphosphonates have. Currently they have only been used in micellular formulations. In the future they will have to be evaluated to see if they have high enough affinity to localize an attached peptide therapeutic. It is likely that a multivalent version will be needed, but the polyphosate multivalent version we tested had poor performance. Work will be needed to design a multivalent version for larger payloads. Considered together with the cumbersome synthesis and poor solubility of bisphosphonates, ranelates, and polyphosphates, we elected to focus all further efforts on the optimization of acidic oligopeptides.

We found that both 10-mers and 20-mers of aspartic acid and glutamic acid were very effective at targeting bone fractures, but some differences did exist. For example, we determined that use of the non-natural D enantiomers of AOPs would increase their retention time on the fracture surface. The biggest difference occurs in retention time. When the relative distribution of the existing drug in the body is compared, the specificity is fairly constant between these groups (see supplemental Figs. 17–20) Retention times can be important, since they will impact how frequently a drug must be re-administered to maintain a therapeutically effective concentration at the fracture site as well as how much of a drug must be given to elicit a response. In the treatment of bone fractures that don't require prolonged hospitalization, for example, less-frequent injections could improve patient compliance.

We also found that glutamic acid and aspartic acid polymers had similar retention times at the fracture site. This confirms the work of others who have shown that they have similar affinities for hydroxyapatite [44]. While oligoaspartic acids might be preferred over oligoglutamic acids for hydroxyapatite targeting because of their reduced nonspecific retention in the kidneys [50], we have found that the slight increase in kidney retention observed with oligoglutamic acid is only transient, and that at time-points longer than 18 h, both oligopeptides nearly quantitatively clear from the kidneys. We have also observed that aspartic acid polymers present a significant synthetic challenge as they can spontaneously form aspartamide impurities [88,89], rendering their eventual manufacturing and purification more problematic than oligoglutamic acids. Potentially of great importance, glutamic acid has been associated with nucleation of hydroxyapatite whereas aspartic acid-rich sequences are responsible for the inhibitory effects observed in osteopontin [98,99].

With the success of oligoglutamic acids as hydroxyapatite-targeting agents now established, the question arises whether other bone components that become exposed primarily after fracture formation might similarly be developed as fracture-targeting ligands. It is clear that collagen mimetic peptides that trimerize with damaged or forming collagen [100,101] or compounds that contain collagen-binding domains can be conjugated to bone anabolic agents in order to improve bone quality and likely fracture repair [20,102]. These techniques are limited, however, by the ubiquitous distribution of collagen in the body and struggle to achieve a high specificity for fractures. Other targets, such as those based on cellular receptors, enable more specific delivery of drugs to the cells responsible for the repair. These could include osteoblast-specific peptides such as SDSDD that binds to osteoblasts via periostin [103] (see supplemental Fig. 12), or osteoclast-specific peptides like Tartrate-resistant acid phosphatase (TRAP) binding peptide [104]. Using the recently-developed TRAP binding peptide to localize drug to the fracture site has only elcited moderate targeting specificity [105,106]. However these alternate non hydroxyapatite-binding techniques could hold promise, assuming that molecular receptors expressed specifically on active osteoblasts or osteoclasts can be found in sufficient numbers for delivery of therapeutic concentrations of payload [107]. Hydroxyapatite targeting is specific to regions of damaged or remodeling bone due to the blood bone barrier [108] and unlike receptor-based targeting, it can localize enormous amounts of compound before saturation is achieved (see supplemental Fig. 21).

Future work in this area will have to evaluate the pharmacological efficacy of anabolics targeted by D-Glu_{20} and the other various bone targeting ligands. Different dosing regiments will have to be evaluated to identify the impacts the improved half-lives have on frequency of dose administration. These compounds can be further optimized and evaluated to see if different chemical modifications can further improve the delivery capacity and specificity of these targeting ligands. In addition, future work should compare these to newer targeting ligands like TRAP binding peptide, and pyrophosphate. The foundation of this work is to build the ground work for better bone fracture targeted drugs and the ultimate goal of this work is to develop and translate a bone targeted therapy for the improvement of bone fracture healing.

In summary, we have found that short oligopeptides of acidic amino acids can localize to bone fractures with high selectivity compared to bisphosphonates and tetracyclines. We have also demonstrated the ability of these AOPs to target peptides of all chemical classes: hydrophobic, neutral, cationic, anionic, short oligopeptides, and long polypeptides. This is particularly useful as many bone anabolic agents are peptidic in nature, but their physical properties vary greatly. After examining the targeting abilities of multiple AOPs, we determined that D-Glu_{20} is an ideal candidate for targeting peptide therapeutics to bone fracture surfaces.

Funding

This work was supported in part by the National Institutes of Health [TL1 TR002531, UL1 TR002529, R44DE028713].

Declaration of Competing Interest

JN, SW, MW, SL– all are co-inventors on patents related to this technology. SL and PL are shareholders of Novosteo INC.

Acknowledgments

We acknowledge the use of the core facilities of the Purdue Imaging Facility, a core facility of the NIH-funded Indiana Clinical and Translational Sciences Institute as well as the Purdue Institute for Drug Discovery. We would also like to acknowledge the laboratory assistance granted by the following individuals: Elena Konrath, Christopher Chen, Ephraim Mbachu, Madeleine Tremblay, Kayleen Nordyke, Gabrielle Selvia, Cheyanne Coakley, and Stephanie Devoe. We acknowledge Jalena Nielsen's assistance in editing the manuscript.

Appendix A. Supplementary data

Supplementary data to this article can be found online at https://doi.

org/10.1016/j.jconrel.2020.09.047.

References

[1] Bone and Joint Initiative, By the numbers: musculoskeletal injuries, Bone Jt. Initiat. (2012), 2012–2013, http://www.boneandjointburden.org/docs/By. The Numbers-MSK Injuries.pdf.

[2] P. Carpintero, J.R. Caeiro, R. Carpintero, A. Morales, S. Silva, M. Mesa, P. Carpintero, R. Carpintero, S. Silva, R. Sofia, Complications of hip fractures: a review, World J. Orthop. 5 (2014) 402–411, https://doi.org/10.5312/wjo.v5.i4.402.

[3] A. Parashar, R.K. Sharma, Unfavourable outcomes in maxillofacial injuries: how to avoid and manage, Indian J. Plast. Surg. 46 (2013) 221–234, https://doi.org/10.4103/0970-0358.118597.

[4] The Bone and Joint Initative, The Burden of Musculoskeletal Diseases in the United States, Fourth ed., Burd. Musculoskelet. Dis., United States, 2019.

[5] R. Gruber, H. Koch, B.A. Doll, F. Tegtmeier, T.A. Einhorn, J.O. Hollinger, Fracture healing in the elderly patient, Exp. Gerontol. 41 (2006) 1080–1093, https://doi.org/10.1016/j.exger.2006.09.008.

[6] G.T.T. Helmerhorst, A.M. Vranceanu, M. Vrahas, M. Smith, D. Ring, Risk factors for continued opioid use one to two months after surgery for musculoskeletal trauma, J. Bone Jt. Surg. Ser. A. 96 (2014) 495–499, https://doi.org/10.2106/JBJS.L.01406.

[7] L.A. Beaupre, C.A. Jones, L.D. Saunders, D.W.C. Johnston, C. Frcs, J. Buckingham, S.R. Majumdar, Best practices for elderly hip fracture patients a systematic overview of the evidence, J. Gen. Intern. Med. 20 (2005) 1019–1025, https://doi.org/10.1111/j.1525-1497.2005.0219.x.

[8] A.R. Poynton, J.M. Lane, Safety profile for the clinical use of bone morphogenetic proteins in the spine, Spine (Phila. Pa.) 27 (2002) (1976) 40–48, https://doi.org/10.1097/00007632-200208151-00010.

[9] T. Jung, J.H. Lee, S. Park, Y.J. Kim, J. Seo, H.E. Shim, K.S. Kim, H.S. Jang, H. M. Chung, S.G. Oh, S.H. Moon, S.W. Kang, Effect of BMP-2 delivery mode on osteogenic differentiation of stem cells, Stem Cells Int. 2017 (2017), https://doi.org/10.1155/2017/7859184.

[10] E. Bergeron, E. Leblanc, O. Drevelle, R. Giguère, S. Beauvais, G. Grenier, N. Faucheux, The evaluation of ectopic bone formation induced by delivery systems for bone morphogenetic protein-9 or its derived peptide, Tissue Eng. - Part A. 18 (2012) 342–352, https://doi.org/10.1089/ten.tea.2011.0008.

[11] A.W. James, G. LaChaud, J. Shen, G. Asatrian, V. Nguyen, X. Zhang, K. Ting, C. Soo, A review of the clinical side effects of bone morphogenetic protein-2, Tissue Eng. Part B Rev. 22 (2016) 284–297, https://doi.org/10.1089/ten.teb.2015.0357.

[12] Albert M. Chung, Calcitonin gene-related peptide (CGRP): role in peripheral nerve regeneration, Rev. Neurosci. 29 (2018) 369, https://doi.org/10.1515/revneuro-2017-0060.

[13] S. Grässel, The role of peripheral nerve fibers and their neurotransmitters in cartilage and bone physiology and pathophysiology, Arthritis Res. Ther. 16 (2014), https://doi.org/10.1186/s13075-014-0485-1.

[14] F. Elefteriou, Neuronal signaling and the regulation of bone remodeling, Cell. Mol. Life Sci. 62 (2005) 2339–2349, https://doi.org/10.1007/s00018-005-5175-3.

[15] C.G.T. Tahimic, Y. Wang, D.D. Bikle, Anabolic effects of IGF-1 signaling on the skeleton, Front. Endocrinol. (Lausanne). 4 (2013) 1–14, https://doi.org/10.3389/fendo.2013.00006.

[16] M.A. Bednarek, S.D. Feighner, S.S. Pong, K.K. McKee, D.L. Hreniuk, M.V. Silva, V. A. Warren, A.D. Howard, L.H.Y. Van der Ploeg, J.V. Heck, Structure - function studies on the new growth hormone-releasing peptide, ghrelin: minimal sequence of ghrelin necessary for activation of growth hormone secretagogue receptor 1a, J. Med. Chem. 43 (2000) 4370–4376, https://doi.org/10.1021/jm0001727.

[17] T.F. Lane, M.L. Iruela-Arispe, R.S. Johnson, E.H. Sage, SPARC is a source of copper-binding peptides that stimulate angiogenesis, J. Cell Biol. 125 (1994) 929–943, https://doi.org/10.1083/jcb.125.4.929.

[18] R. DiStasi, D. Diana, D. Capasso, S. DiGaetano, L. DeRosa, V. Celentano, C. Isernia, R. Fattorusso, L.D. D'Andrea, VEGFR recognition interface of a proangiogenic VEGF-mimetic peptide determined *in vitro* and in the presence of endothelial cells by NMR spectroscopy, Chem. Eur. J. (2018) 11461–11466, https://doi.org/10.1002/chem.201802117.

[19] A. Verheyen, E. Peeraer, D. Lambrechts, K. Poesen, P. Carmeliet, M. Shibuya, I. Pintelon, J.P. Timmermans, R. Nuydens, T. Meert, Therapeutic potential of VEGF and VEGF-derived peptide in peripheral neuropathies, Neuroscience 244 (2013) 77–89, https://doi.org/10.1016/j.neuroscience.2013.03.050.

[20] T. Ponnapakkam, R. Katikaneni, J. Sakon, R. Stratford, R.C. Gensure, Treating osteoporosis by targeting parathyroid hormone to bone, Drug Discov. Today 19 (2014) 204–208, https://doi.org/10.1016/j.drudis.2013.07.015.

[21] R. Brommage, C.E. Hotchkiss, C.J. Lees, M.W. Stancill, J.M. Hock, C.P. Jerome, Daily treatment with human recombinant parathyroid hormone-(1-34), LY333334, for 1 year increases bone mass in ovariectomized monkeys, J. Clin. Endocrinol. Metab. 84 (1999) 3757–3763, https://doi.org/10.1210/jc.84.10.3757.

[22] N. Shaikh, L. Russo, E. Papaleo, P. Giannoni, L. De Gioia, F. Nicotra, R. Quarto, L. Cipolla, C-type natriuretic peptide: structural studies, fragment synthesis, and preliminary biological evaluation in human osteosarcoma cell lines, Biopolymers 94 (2010) 213–219, https://doi.org/10.1002/bip.21336.

[23] A.V. Haas, M.S. LeBoff, Osteoanabolic agents for osteoporosis, J. Endocr. Soc. 2 (2018) 922–932, https://doi.org/10.1210/js.2018-00118.

[24] R. Health, A randomized, double-blind, placebo-controlled, comparative phase 3 multicenter study to evaluate the safety and efficacy of BA058 for injection for prevention of fracture in ambulatory postmenopausal women with severe osteoporosis and at risk of fracture, JAMA (2011), https://doi.org/10.1002/central/CN-01841784/full.

[25] J.B. Ziffra, B. Olshansky, Teriparatide-induced atrial tachycardia, BMJ Case Rep. 2018 (2018) 2017–2018, https://doi.org/10.1136/bcr-2017-223035.

[26] M.S. Nieminen, M.P. Ramo, M. Viitasalo, P. Heikkila, J. Karjalainen, M. Mantysaari, J. Heikkila, Serious cardiovascular side effects of large doses of anabolic steroids in weight lifters, Eur. Heart J. 17 (1996) 1576–1583, https://doi.org/10.1093/oxfordjournals.eurheartj.a014724.

[27] M. Yuasa, T. Yamada, T. Taniyama, T. Masaoka, W. Xuetao, T. Yoshii, M. Horie, H. Yasuda, T. Uemura, A. Okawa, S. Sotome, Dexamethasone enhances osteogenic differentiation of bone marrow-and muscle-derived stromal cells and augments ectopic bone formation induced by bone morphogenetic protein-2, PLoS One 10 (2015) 1–23, https://doi.org/10.1371/journal.pone.0116462.

[28] C.H. Kim, S.L. Cheng, G.S. Kim, Effects of dexamethasone on proliferation, activity, and cytokine secretion of normal human bone marrow stromal cells: possible mechanisms of glucocorticoid-induced bone loss, J. Endocrinol. 162 (1999) 371–379, https://doi.org/10.1677/joe.0.1620371.

[29] M.I. Antczak, Y. Zhang, C. Wang, J. Doran, J. Naidoo, S. Voruganti, N.S. Williams, S.D. Markowitz, J.M. Ready, Inhibitors of 15-prostaglandin dehydrogenase to potentiate tissue repair, J. Med. Chem. 60 (2017) 3979–4001, https://doi.org/10.1021/acs.jmedchem.7b00271.

[30] Y. Zhang, A. Desai, S.Y. Yang, K.B. Bae, M.I. Antczak, S.P. Fink, S. Tiwari, J. E. Willis, N.S. Williams, D.M. Dawson, D. Wald, W.D. Chen, Z. Wang, L. Kasturi, G.A. Larusch, L. He, F. Cominelli, L. Di Martino, Z. Djuric, G.L. Milne, M. Chance, J. Sanabria, C. Dealwis, D. Mikkola, J. Naidoo, S. Wei, H.H. Tai, S.L. Gerson, J. M. Ready, B. Posner, J.K.V. Willson, S.D. Markowitz, Inhibition of the prostaglandin-degrading enzyme 15-PGDH potentiates tissue regeneration, Science 348 (2015), https://doi.org/10.1126/science.aaa2340.

[31] D.C. Beachler, E.L. Yanik, B.I. Martin, R.M. Pfeiffer, S.K. Mirza, R.A. Deyo, E. A. Engels, Bone morphogenetic protein use and cancer risk among patients undergoing lumbar arthrodesis a case-cohort study using the SEER-medicare database, J. Bone Jt. Surg. Am. 98 (2016) 1064–1072, https://doi.org/10.2106/JBJS.15.01106.

[32] A. Gilsenan, A. Harding, N. Kellier-Steele, D. Harris, K. Midkiff, E. Andrews, The Forteo patient registry linkage to multiple state cancer registries: study design and results from the first 8 years, Osteoporos. Int. 29 (2018) 2335–2343, https://doi.org/10.1007/s00198-018-4604-8.

[33] M. Stapleton, K. Sawamoto, C.J. Alméciga-Díaz, W.G. Mackenzie, R.W. Mason, T. Orii, S. Tomatsu, Development of bone targeting drugs, Int. J. Mol. Sci. 18 (2017) 1–15, https://doi.org/10.3390/ijms18071345.

[34] L.E. Cole, T. Vargo-gogola, R.K. Roeder, Targeted Delivery to Bone and Mineral Deposits Using Bisphosphonate Ligands, Elsevier B.V., 2016, https://doi.org/10.1016/j.addr.2015.10.005.

[35] R. Bergmann, M. Meckel, V. Kubíček, J. Pietzsch, J. Steinbach, P. Hermann, F. Rösch, 177Lu-labelled macrocyclic bisphosphonates for targeting bone metastasis in cancer treatment, EJNMMI Res. 6 (2016) 1–12, https://doi.org/10.1186/s13550-016-0161-3.

[36] H. Xie, G. Chen, R.N. Young, Design, Synthesis, and Pharmacokinetics of a Bone-Targeting Dual-Action Prodrug for the Treatment of Osteoporosis, 2017, https://doi.org/10.1021/acs.jmedchem.6b00951.

[37] P.P. Sedghizadeh, S. Sun, A.F. Junka, E. Richard, K. Sadrerafi, S. Mahabady, N. Bakhshalian, N. Tjokro, M. Bartoszewicz, M. Oleksy, P. Szymczyk, M. W. Lundy, J.D. Neighbors, R.G.G. Russell, C.E. McKenna, F.H. Ebetino, Design, Synthesis, and Antimicrobial Evaluation of a Novel Bone-Targeting Bisphosphonate-Ciprofloxacin Conjugate for the Treatment of Osteomyelitis Biofilms, 2017, https://doi.org/10.1021/acs.jmedchem.6b01615.

[38] R.N. Young, M.D. Grynpas, Targeting therapeutics to bone by conjugation with bisphosphonates, Curr. Opin. Pharmacol. 40 (2018) 87–94, https://doi.org/10.1016/j.coph.2018.03.010.

[39] V. Hengst, C. Oussoren, T. Kissel, G. Storm, Bone targeting potential of bisphosphonate-targeted liposomes. Preparation, characterization and hydroxyapatite binding *in vitro*, Int. J. Pharm. 331 (2007) 224–227, https://doi.org/10.1016/j.ijpharm.2006.11.024.

[40] J.R. Neale, N.B. Richter, K.E. Merten, K.G. Taylor, S. Singh, L.C. Waite, N. K. Emery, N.B. Smith, J. Cai, W.M. Pierce, Bioorganic & medicinal chemistry letters bone selective effect of an estradiol conjugate with a novel tetracycline-derived bone-targeting agent, Bioorg. Med. Chem. Lett. 19 (2009) 680–683, https://doi.org/10.1016/j.bmcl.2008.12.051.

[41] G. Chai, F. Hu, Tetracycline-grafted PLGA nanoparticles as bone-targeting drug delivery system, Int. J. Nanomed. 10 (2015) 5671–5685.

[42] S.C. Miller, H. Pan, D. Wang, B.M. Bowman, P. Kopečková, J. Kopeček, Feasibility of using a bone-targeted, macromolecular delivery system coupled with prostaglandin E1 to promote bone formation in aged, estrogen-deficient rats, Pharm. Res. 25 (2008) 2889–2895, https://doi.org/10.1007/s11095-008-9706-0.

[43] J. Ishizaki, Y. Waki, T. Takahashi-Nishioka, K. Yokogawa, K.I. Miyamoto, Selective drug delivery to bone using acidic oligopeptides, J. Bone Miner. Metab. (2009), https://doi.org/10.1007/s00774-008-0004-z.

[44] T. Sekido, N. Sakura, Y. Higashi, K. Miya, Y. Nitta, M. Nomura, H. Sawanishi, K. Morito, Y. Masamune, S. Kasugai, K. Yokogawa, K.I. Miyamoto, Novel drug delivery system to bone using acidic oligopeptide: pharmacokinetic characteristics and pharmacological potential, J. Drug Target. (2001), https://doi.org/10.3109/10611860108997922.

[45] E.J. Carbone, K. Rajpura, T. Jiang, H.M. Kan, X. Yu, K.W.H. Lo, Osteotropic nanoscale drug delivery system via a single aspartic acid as the bone-targeting moiety, J. Nanosci. Nanotechnol. 17 (2017) 1747–1752, https://doi.org/10.1166/jnn.2017.12855.

[46] K. Vincent, M.C. Durrant, Journal of Molecular Graphics and Modelling a Structural and Functional Model for Human Bone Sialoprotein, Elsevier Inc., 2013, https://doi.org/10.1016/j.jmgm.2012.10.007.

[47] T. Takahashi, K. Yokogawa, N. Sakura, M. Nomura, S. Kobayashi, K.I. Miyamoto, Bone-targeting of quinolones conjugated with an acidic oligopeptide, Pharm. Res. 25 (2008) 2881–2888, https://doi.org/10.1007/s11095-008-9605-4.

[48] S.A. Low, J. Kopeček, Targeting polymer therapeutics to bone, Adv. Drug Deliv. Rev. 64 (2012) 1189–1204, https://doi.org/10.1016/j.addr.2012.01.012.

[49] T.J. Houghton, K.S.E. Tanaka, T. Kang, E. Dietrich, Y. Lafontaine, D. Delorme, S. S. Ferreira, F. Viens, F.F. Arhin, I. Sarmiento, D. Lehoux, I. Fadhil, K. Laquerre, J. Liu, V. Ostiguy, H. Poirier, G. Moeck, T.R. Parr, A.R. Far, Linking bisphosphonates to the free amino groups in fluoroquinolones: preparation of osteotropic prodrugs for the prevention of osteomyelitis, J. Med. Chem. 51 (2008) 6955–6969, https://doi.org/10.1021/jm801007z.

[50] K. Ogawa, A. Ishizaki, K. Takai, Y. Kitamura, A. Makino, T. Kozaka, Y. Kiyono, K. Shiba, A. Odani, Evaluation of Ga-DOTA-(D-asp)n as bone imaging agents: D-aspartic acid peptides as carriers to bone, Sci. Rep. 7 (2017) 1–11, https://doi.org/10.1038/s41598-017-14149-7.

[51] K.B. Farrell, A. Karpeisky, D.H. Thamm, S. Zinnen, Bisphosphonate Conjugation for Bone Specific Drug Targeting, Elsevier, 2018, https://doi.org/10.1016/j.bonr.2018.06.007.

[52] H. Wang, L. Xiao, J. Tao, V. Srinivasan, B.F. Boyce, F.H. Ebetino, B.O. Oyajobi, R. K. Boeckman, L. Xing, Synthesis of a bone-targeted bortezomib with in vivo anti-myeloma effects in mice, Pharmaceutics 10 (2018) 1–13, https://doi.org/10.3390/pharmaceutics10030154.

[53] C.C. Liu, S. Hu, G. Chen, J. Georgiou, S. Arns, N.S. Kumar, R.N. Young, M. D. Grynpas, Novel EP4 receptor agonist-bisphosphonate conjugate drug (C1) promotes bone formation and improves vertebral mechanical properties in the ovariectomized rat model of postmenopausal bone loss, J. Bone Miner. Res. 30 (2015) 670–680, https://doi.org/10.1002/jbmr.2382.

[54] S. Arns, R. Gibe, A. Moreau, M. Monzur Morshed, R.N. Young, Design and synthesis of novel bone-targeting dual-action pro-drugs for the treatment and reversal of osteoporosis, Bioorg. Med. Chem. 20 (2012) 2131–2140, https://doi.org/10.1016/j.bmc.2012.01.024.

[55] M. Morioka, A. Kamizono, H. Takikawa, A. Mori, H. Ueno, S. Ichiro Kadowaki, Y. Nakao, K. Kato, K. Umezawa, Design, synthesis, and biological evaluation of novel estradiol-bisphosphonate conjugates as bone-specific estrogens, Bioorg. Med. Chem. 18 (2010) 1143–1148, https://doi.org/10.1016/j.bmc.2009.12.041.

[56] D. Wang, S.C. Miller, L.S. Shlyakhtenko, A.M. Portillo, X.-M. Liu, K. Papangkorn, P. Kopecková, Y. Lyubchenko, W.I. Higuchi, J. Kopecek, Osteotropic Peptide that differentiates functional domains of the skeleton, Bioconjug. Chem. 18 (2007) 1375–1378, https://doi.org/10.1021/bc7002132.

[57] S.A. Low, C.V. Galliford, J. Yang, P.S. Low, S.L. City, P. Chemistry, S.L. City, W. Lafayette, Biodistribution of fracture-targeted GSK3β inhibitor-loaded micelles for improved fracture healing, Biomacromolecules (2015), https://doi.org/10.1021/acs.biomac.5b00777.Biodistribution.

[58] M. Wang, S. Park, Y. Nam, J. Nielsen, S.A. Low, M. Srinivasarao, P.S. Low, Bone-fracture-targeted Dasatinib-Oligoaspartic acid conjugate potently accelerates fracture repair, Bioconjug. Chem. 29 (2018) 3800–3809, https://doi.org/10.1021/acs.bioconjchem.8b00660.

[59] S.A. Low, C.V. Galliford, Y.L. Jones-Hall, J. Roy, J. Yang, P.S. Low, J. Kopeček, Healing efficacy of fracture-targeted GSK3β inhibitor-loaded micelles for improved fracture repair, Nanomedicine 12 (2017) 185–193, https://doi.org/10.2217/nnm-2016-0340.

[60] S.G. Rotman, D.W. Grijpma, R.G. Richards, T.F. Moriarty, D. Eglin, O. Guillaume, Drug Delivery Systems Functionalized with Bone Mineral Seeking Agents for Bone Targeted Therapeutics, Elsevier, 2018, https://doi.org/10.1016/j.jconrel.2017.11.009.

[61] M. Stapleton, K. Sawamoto, C.J. Alméciga-Díaz, W.G. Mackenzie, R.W. Mason, T. Orii, S. Tomatsu, Development of bone targeting drugs, J. Mol. Sci. (2017), https://doi.org/10.3390/ijms18071345.

[62] J.J. Nielsen, S.A. Low, Bone targeting systems to systemically deliver therapeutics to bone fractures for accelerated healing, Curr. Osteoporsis Reportssteoporsis Reports (2020) 449–459.

[63] C.P. Leamon, M.A. Parker, I.R. Vlahov, L.C. Xu, J.A. Reddy, M. Vetzel, N. Douglas, Synthesis and biological evaluation of EC20: a new folate-derived, 99mTc-based radiopharmaceutical, Bioconjug. Chem. 13 (2002) 1200–1210, https://doi.org/10.1021/bc0200430.

[64] J.C. Savoie, P. Thomopoulos, F. Savoie, Studies on mono- and diiodohistidine. I. The identification of iodohistidines from thyroidal iodoproteins and their peripheral metabolism in the normal man and rat, J. Clin. Invest. 52 (1973) 106–115, https://doi.org/10.1172/JCI107153.

[65] D.M. Chauncey, S.E. Halpern, P.L. Hagan, N.P. Alazraki, Tumor model studies of 131I-tetracycline and other compounds, J. Nucl. Med. 17 (1976) 274–281.

[66] D.D. Perrin, Binding of Tetracyclines to bone, Nature 208 (1965) 787–788, https://doi.org/10.1038/208787a0.

[67] B. Halling-Sørensen, G. Sengeløv, J. Tjørnelund, Toxicity of tetracyclines and tetracycline degradation products to environmentally relevant bacteria, including selected tetracycline-resistant bacteria, Arch. Environ. Contam. Toxicol. 42 (2002) 263–271, https://doi.org/10.1007/s00244-001-0017-2.

[68] S.T. Cutbirth, A restorative challenge: tetracycline-stained teeth, Denistry Today (2015) 3–6.

[69] C. Wang, Y. Liu, Y. Fan, X. Li, The use of bioactive peptides to modify materials for bone tissue repair, Regen. Biomater. 4 (2017) 191–206, https://doi.org/10.1093/rb/rbx011.

[70] O.H. Jeon, J. Elisseeff, Orthopedic Tissue Regeneration: Cells, Scaffolds, and Small Molecules, 2016, https://doi.org/10.1007/s13346-015-0266-7.

[71] R. Visser, G.A. Rico-Llanos, H. Pulkkinen, J. Becerra, Peptides for Bone Tissue Engineering, Elsevier B.V., 2016, https://doi.org/10.1016/j.jconrel.2016.10.024.

[72] T. Sibai, E.F. Morgan, T.A. Einhorn, Anabolic agents and bone quality, Clin. Orthop. Relat. Res. 469 (2011) 2215–2224, https://doi.org/10.1007/s11999-010-1722-9.

[73] Z. Amso, J. Cornish, M.A. Brimble, Short anabolic peptides for bone growth, Med. Res. Rev. 36 (2016) 579–640, https://doi.org/10.1002/med.

[74] E.J. Campbell, G.M. Campbell, D.A. Hanley, The effect of parathyroid hormone and teriparatide on fracture healing, Expert. Opin. Biol. Ther. 15 (2015) 119–129, https://doi.org/10.1517/14712598.2015.977249.

[75] S.H. Choi, J.N.R. Collins, S.A. Smith, R.L. Davis-Harrison, C.M. Rienstra, J. H. Morrissey, Phosphoramidate end labeling of inorganic polyphosphates: facile manipulation of polyphosphate for investigating and modulating its biological activities, Biochemistry 49 (2010) 9935–9941, https://doi.org/10.1021/bi1014437.

[76] Y. Hacchou, T. Uematsu, O. Ueda, Y. Usui, S. Uematsu, M. Takahashi, T. Uchihashi, Y. Kawazoe, T. Shiba, S. Kurihara, M. Yamaoka, K. Furusawa, Inorganic polyphosphate: a possible stimulant of bone formation, J. Dent. Res. 86 (2007) 893–897, https://doi.org/10.1177/154405910708600917.

[77] J.P. Brown, S. Morin, M.W. Leslie, A. Papaioannou, A.M. Cheung, K.S. Davison, D. Goltzman, D.A. Hanley, A. Hodsman, R. Josse, A. Jovaisas, A. Juby, S. Kaiser, A. Karaplis, D. Kendler, A. Khan, D. Ngui, W. Olszynski, L.G. Ste-Marie, J. Adachi, Bisphosphonates for treatment of osteoporosis: expected benefits, potential harms, and drug holidays, Can. Fam. Physician 60 (2014) 324–333.

[78] Z. Amso, J. Cornish, M.A. Brimble, Short anabolic peptides for bone growth, Med. Res. Rev. 36 (2016) 579–640, https://doi.org/10.1002/med.

[79] H. Shin, K. Zygourakis, M.C. Farach-carson, M.J. Yaszemski, A.G. Mikos, Attachment, proliferation, and migration of marrow stromal osteoblasts cultured on biomimetic hydrogels modified with an osteopontin-derived peptide, Biomaterials 25 (2004) 895–906, https://doi.org/10.1016/S0142-9612(03)00602-1.

[80] V. Agrawal, D. Ph, J. Kelly, D. Ph, S. Tottey, D. Ph, K.A. Daly, D. Ph, S.A. Johnson, B.F. Siu, J. Reing, An isolated cryptic peptide influences osteogenesis and bone Remodeling in an adult mammalian model of digit amputation, Tissue Eng. Part A. 17 (2011) 3033–3044, https://doi.org/10.1089/ten.tea.2011.0257.

[81] V. Agrawal, S. Tottey, D. Ph, S.A. Johnson, J.M. Freund, B.F. Siu, S.F. Badylak, D. Ph, Recruitment of progenitor cells by an extracellular matrix cryptic peptide in a mouse model of digit amputation, Tissue Eng. Part A. 17 (2011) 2435–2444, https://doi.org/10.1089/ten.tea.2011.0036.

[82] H. Senta, E. Bergeron, O. Drevelle, H. Park, N. Faucheux, Combination of synthetic peptides derived from bone morphogenetic proteins and biomaterials for medical applications, Can. J. Chem. Eng. 89 (2011) 227–239, https://doi.org/10.1002/cjce.20453.

[83] M. Li, M.J. Mondrinos, X. Chen, M.R. Gandhi, F.K. Ko, P.I. Lelkes, Elastin blends for tissue engineering scaffolds, J. Biomed. Mater. Res. Part A. 79 (2006) 963–973, https://doi.org/10.1002/jbm.a.

[84] J.-Y. Lee, J.-E. Choo, Y.-S. Choi, K.-Y. Lee, D.-S. Min, S.-H. Pi, Y.-J. Seol, S.-J. Lee, I.-H. Jo, C.-P. Chung, 2 Yoon-Jeong Park1, characterization of the surface immobilized synthetic heparin binding domain derived from human fibroblast growth factor-2 and its effect on osteoblast differentiation, J. Biomed. Mater. Res. Part A. 83 (2007) 963–973, https://doi.org/10.1002/jbm.a.

[85] T. Juhász, C. Matta, É. Katona, C. Somogyi, R. Takács, Pituitary adenylate cyclase-activating polypeptide (PACAP) signalling enhances osteogenesis in UMR-106 cell line, J. Mol. Neurosci. 54 (2014) 555–573, https://doi.org/10.1007/s12031-014-0389-1.

[86] V.A. Uchtman, Structural investigations of calcium binding molecules. II. The crystal and molecular structures of calcium dihydrogen ethane-1-hydroxy-1,1-diphosphonate dihydrate, CaC(CH3)(OH)(PO3H)2·2H2O; implications for polynuclear complex formation, J. Phys. Chem. 76 (1972) 1304–1310, https://doi.org/10.1021/j100653a014.

[87] M. Tavafoghi, M. Cerruti, The role of amino acids in hydroxyapatite mineralization, J. R. Soc. Interface 13 (2016) 20160462, https://doi.org/10.1098/rsif.2016.0462.

[88] J. Ruczynski, B. Lewandowska, P. Mucha, P. Rekowski, Problem of aspartimide formation in Fmoc-based solid-phase peptide synthesis using Dmab group to protect side chain of aspartic acid Jarosław, J. Pept. Sci. (2008) 335–341, https://doi.org/10.1002/psc.

[89] J.P. Tam, M.W. Riemen, R.B. Merrifield, Mechanisms of aspartimide formation: the effects of protecting groups, acid, base, temperature and time, Pept. Res. 1 (1988) 6–18.

[90] J. Shaji, V. Patole, Oral protein and peptide drug delivery, Indian J. Pharm. Sci. 70 (2005) 189–200, https://doi.org/10.1002/0471475734.ch10.

[91] K.S. Ingersoll, J. Cohen, The impact of medication regimen factors on adherence to chronic treatment: a review of literature, J. Behav. Med. 31 (2008) 213–224, https://doi.org/10.1007/s10865-007-9147-y.

[92] C.I. Coleman, B. Limone, D.M. Sobieraj, S. Lee, M.S. Roberts, R. Kaur, T. Alam, Dosing frequency and medication adherence in chronic disease, J. Manag. Care Pharm. 18 (2012) 527–539, https://doi.org/10.18553/jmcp.2012.18.7.527.

[93] M. Kar, S. Singh, S. Singh, D.K. Jain, D.K. Jain, Skeletal drug delivery system: a review, J. Drug Deliv. Ther. 4 (2014) 60–68, https://doi.org/10.22270/jddt.v4i3.836.

[94] K.B. Farrell, A. Karpeisky, D.H. Thamm, S. Zinnen, Bisphosphonate conjugation for bone specific drug targeting, Bone Reports 9 (2018) 47–60, https://doi.org/10.1016/j.bonr.2018.06.007.
[95] L.E. Cole, T. Vargo-Gogola, R.K. Roeder, Targeted delivery to bone and mineral deposits using bisphosphonate ligands, Adv. Drug Deliv. Rev. 99 (2016) 12–27, https://doi.org/10.1016/j.addr.2015.10.005.
[96] M.R.A. Young, J.H. Lowry, J.D. Laird, W.R. Ferguson, 99Tcm-MDP bone scanning of injuries of the carpal scaphoid, Injury 19 (1988) 14–17, https://doi.org/10.1016/0020-1383(88)90166-0.
[97] Y. Liu, Z. Jia, M.P. Akhter, X. Gao, X. Wang, X. Wang, G. Zhao, X. Wei, Y. Zhou, X. Wang, C.W. Hartman, E.V. Fehringer, L. Cui, D. Wang, Bone-targeting liposome formulation of salvianic acid a accelerates the healing of delayed fracture Union in Mice, nanomedicine nanotechnology, Biol. Med. 14 (2018) 2271–2282, https://doi.org/10.1016/j.nano.2018.07.011.
[98] G.K. Hunter, C.L. Kyle, H.A. Goldberg, Modulation of crystal formation by bone phosphoproteins: structural specificity of the osteopontin-mediated inhibition of hydroxyapatite formation, Biochem. J. 300 (1994) 723–728, https://doi.org/10.1042/bj3000723.
[99] G.K. Hunter, H.A. Goldberg, Modulation of crystal formation by bone phosphoproteins: role of glutamic acid-rich sequences in the nucleation of hydroxyapatite by bone sialoprotein, Biochem. J. 302 (Pt 1) (1994) 175–179, https://doi.org/10.1042/bj3020175.
[100] S. Michael Yua, Y. Lib, D. Kim, Collagen mimetic peptides: progress towards functional applications, Soft Matter 7 (2011) 7927–7938, https://doi.org/10.1016/j.physbeh.2017.03.040.
[101] Y. Li, X. Mo, D. Kim, S.M. Yu, Template-tethered collagen mimetic peptides for studying heterotrimeric triple-helical interactions, Biopolymers 95 (2011) 94–104, https://doi.org/10.1002/bip.21536.
[102] T. Ponnapakkam, R. Katikaneni, E. Miller, A. Ponnapakkam, S. Hirofumi, S. Miyata, L.J. Suva, J. Sakon, O. Matsushita, R.C. Gensure, Monthly administration of a novel PTH-collagen binding domain fusion protein is anabolic in mice, Calcif. Tissue Int. 88 (2011) 511–520, https://doi.org/10.1007/s00223-011-9485-1.
[103] Y. Sun, X. Ye, M. Cai, X. Liu, J. Xiao, C. Zhang, Y. Wang, L. Yang, J. Liu, S. Li, C. Kang, B. Zhang, Q. Zhang, Z. Wang, A. Hong, X. Wang, Osteoblast-targeting-peptide modified nanoparticle for siRNA/microRNA delivery, ACS Nano 10 (2016) 5759–5768, https://doi.org/10.1021/acsnano.5b07828.
[104] Y. Wang, M.R. Newman, M. Ackun-farmmer, P. Michael, T. Sheu, J.E. Puzas, D.S. W. Benoit, Fracture-targeted delivery of β-catenin agonists via peptide-functionalized nanoparticles augments fracture healing, ACS Nano (2017), https://doi.org/10.1021/acsnano.7b05103.
[105] Y. Wang, M.R. Newman, M. Ackun-Farmmer, M.P. Baranello, T.J. Sheu, J. E. Puzas, D.S.W. Benoit, Fracture-targeted delivery of β-catenin agonists via peptide-functionalized nanoparticles augments fracture healing, ACS Nano 11 (2017) 9445–9458, https://doi.org/10.1021/acsnano.7b05103.
[106] M.R. Newman, S.G. Russell, C.S. Schmitt, I.A. Marozas, T.J. Sheu, J.E. Puzas, D.S. W. Benoit, Multivalent presentation of peptide targeting groups alters polymer biodistribution to target tissues, Biomacromolecules 19 (2018) 71–84, https://doi.org/10.1021/acs.biomac.7b01193.
[107] M. Srinivasarao, P.S. Low, Ligand-targeted drug delivery, Chem. Rev. 117 (2017) 12133–12164, https://doi.org/10.1021/acs.chemrev.7b00013.
[108] J.E. Shea, S.C. Miller, Skeletal function and structure: implications for tissue-targeted therapeutics, Adv. Drug Deliv. Rev. 57 (2005) 945–957, https://doi.org/10.1016/j.addr.2004.12.017.